

# GRAVITATIONAL LENSING

COSMIC SHEAR I

---

*R. Benton Metcalf*  
2022-2023

# GALAXY-GALAXY LENSING

---

*Individual galaxies rarely have a background galaxy close enough that the lensing shear can be distinguished from the intrinsic shape of the galaxy.*

*However, we might hope to determine the average mass distribution around a particular type of galaxy by **stacking**.*

$$\Delta\Sigma(r) \equiv \bar{\kappa}(r) - \langle\kappa\rangle(r) \simeq \frac{1}{N} \sum_{r-\delta < |x_i - y_j| < r+\delta} \epsilon_t^i \quad \begin{matrix} \text{tangential shear} \\ \text{a distance } r \text{ from "lens" galaxy} \end{matrix}$$

*Because the sources and lenses are at all different distances this is often rescaled to a standard source and lens redshift and the result given as a function of the physical size on the lens plane.*

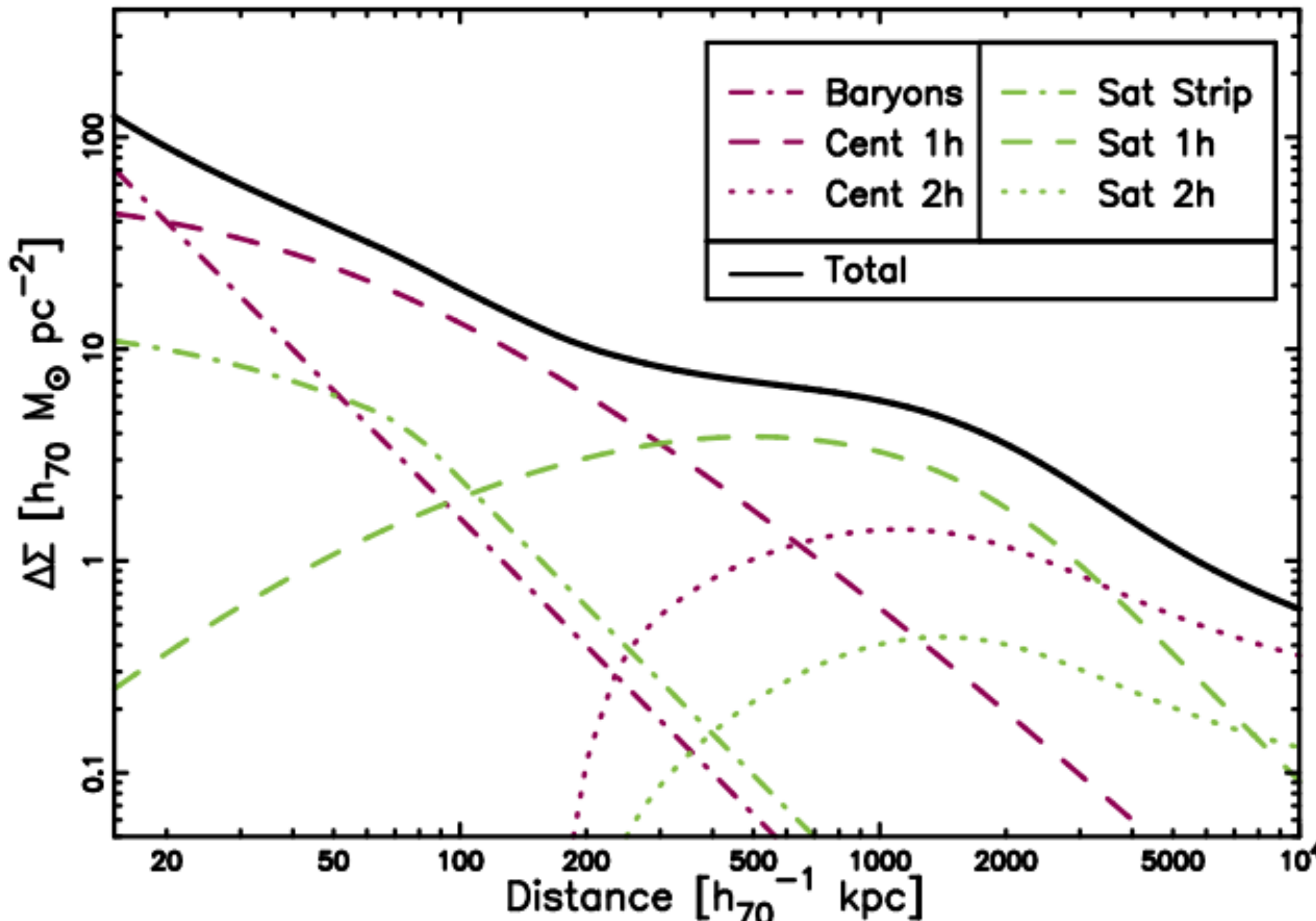
$$\Delta\Sigma(R) \simeq \frac{1}{N\Sigma(\bar{z}_l, \bar{z}_s)} \sum_{R-\delta < |x_i - y_j| D_s < R+\delta} \epsilon_t^i \Sigma_{\text{crit}}(z_i, z_j)$$

*In addition the shear can be weighted to maximise signal-to-noise.*

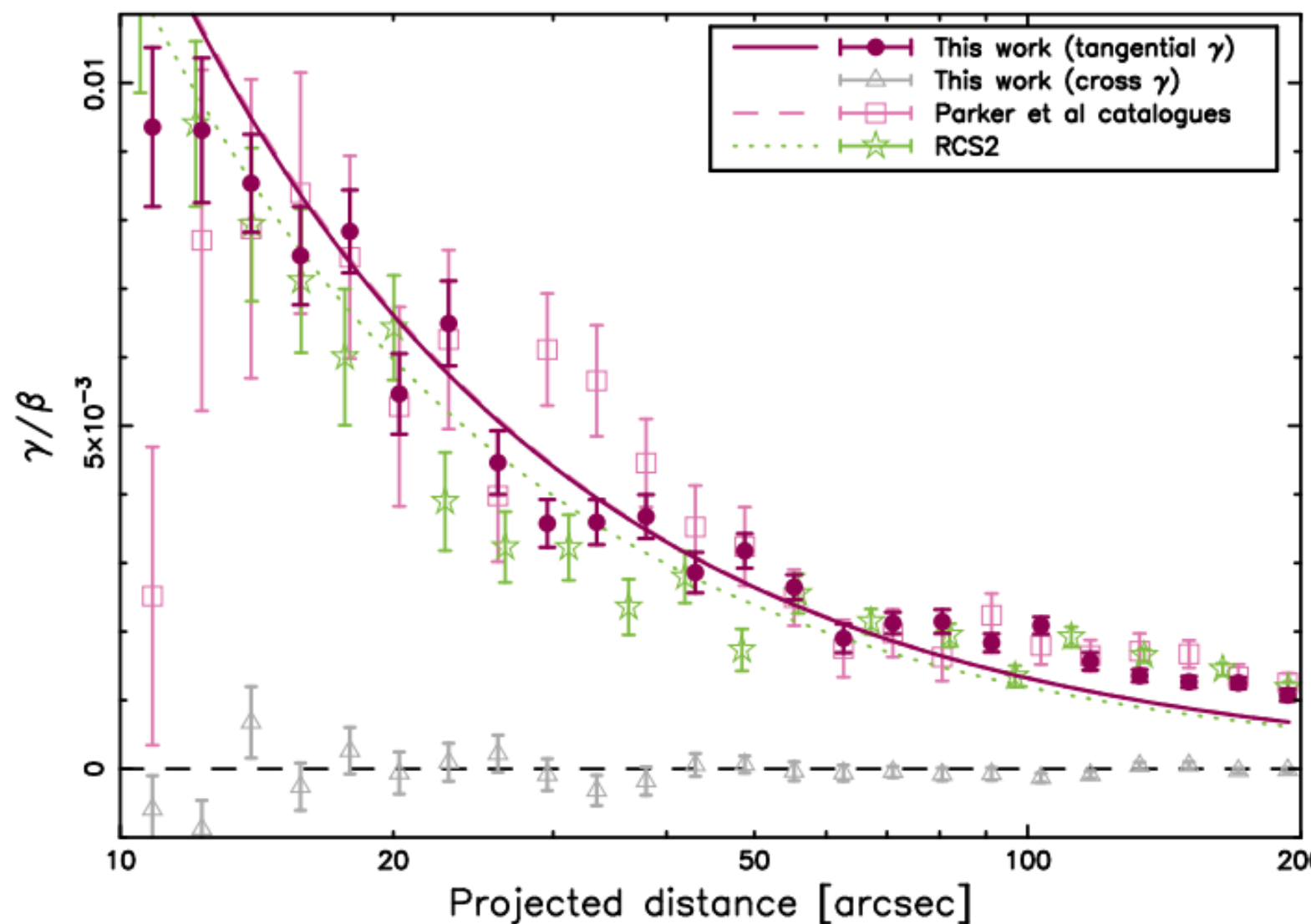
# GALAXY-GALAXY LENSING

*Contributions to the density contrast from stars & dark matter of the lens galaxy and "satellite" galaxies.*

*Velander, et al. 2021*



**Figure 3.** Illustration of the halo model used in this paper. Here we have used a halo mass of  $M_{200} = 10^{12} h_{70}^{-1} M_\odot$ , a stellar mass of  $M_* = 5 \times 10^{10} h_{70}^{-2} M_\odot$  and a satellite fraction of  $\alpha = 0.2$ . The lens redshift is  $z_{\text{lens}} = 0.5$ . Dark purple lines represent quantities tied to galaxies which are centrally located in their haloes while light green lines correspond to satellite quantities. The dark purple dash-dotted line is the baryonic component, the light green dash-dotted line is the stripped satellite halo, dashed lines are the 1-halo components induced by the main dark matter halo and dotted lines are the 2-halo components originating from nearby haloes.

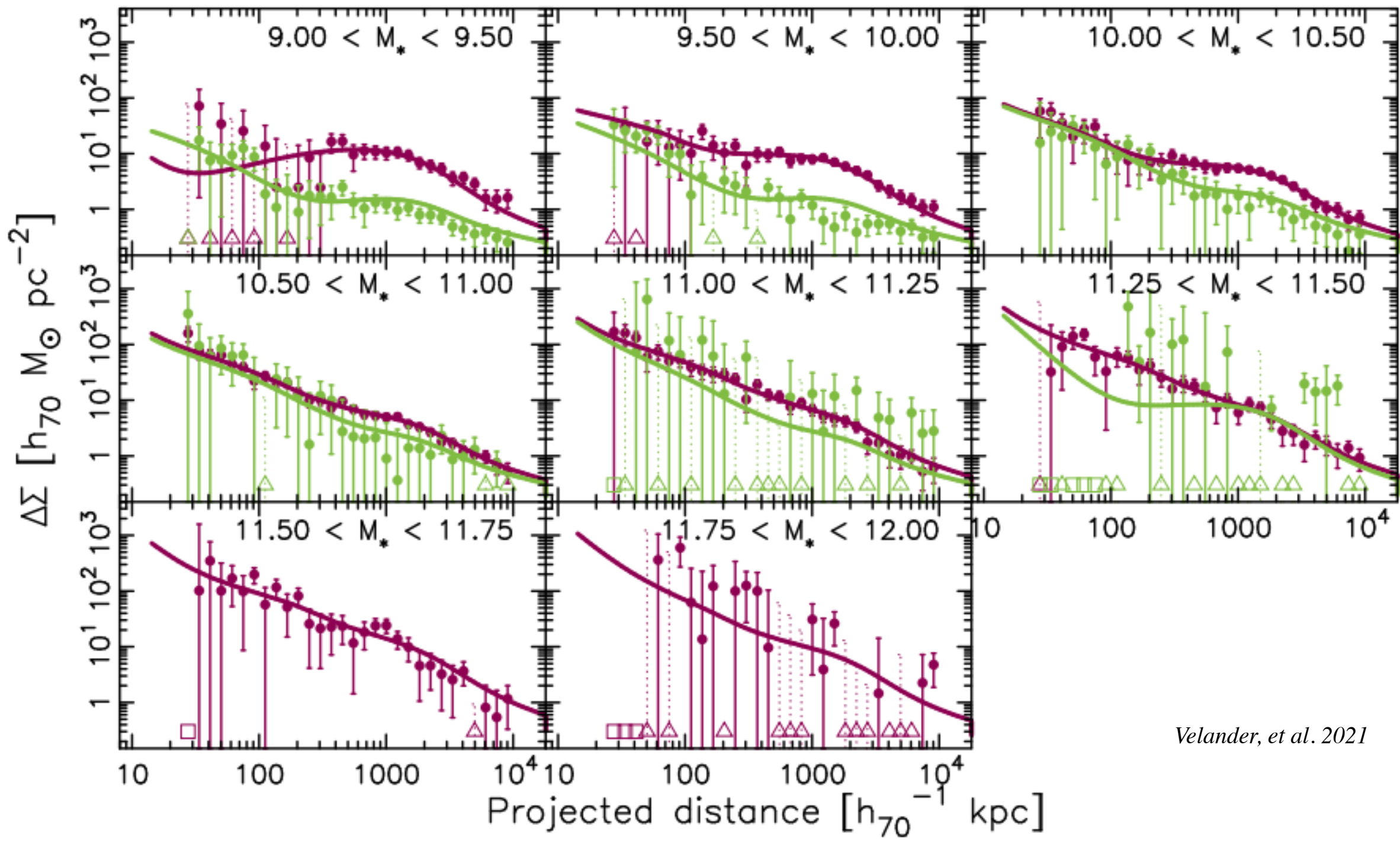
24 *CFHTLenS*

Velander, et al. 2021

# GALAXY-GALAXY LENSING

*CFHTLenS: Relation between galaxy DM haloes and baryons*

11

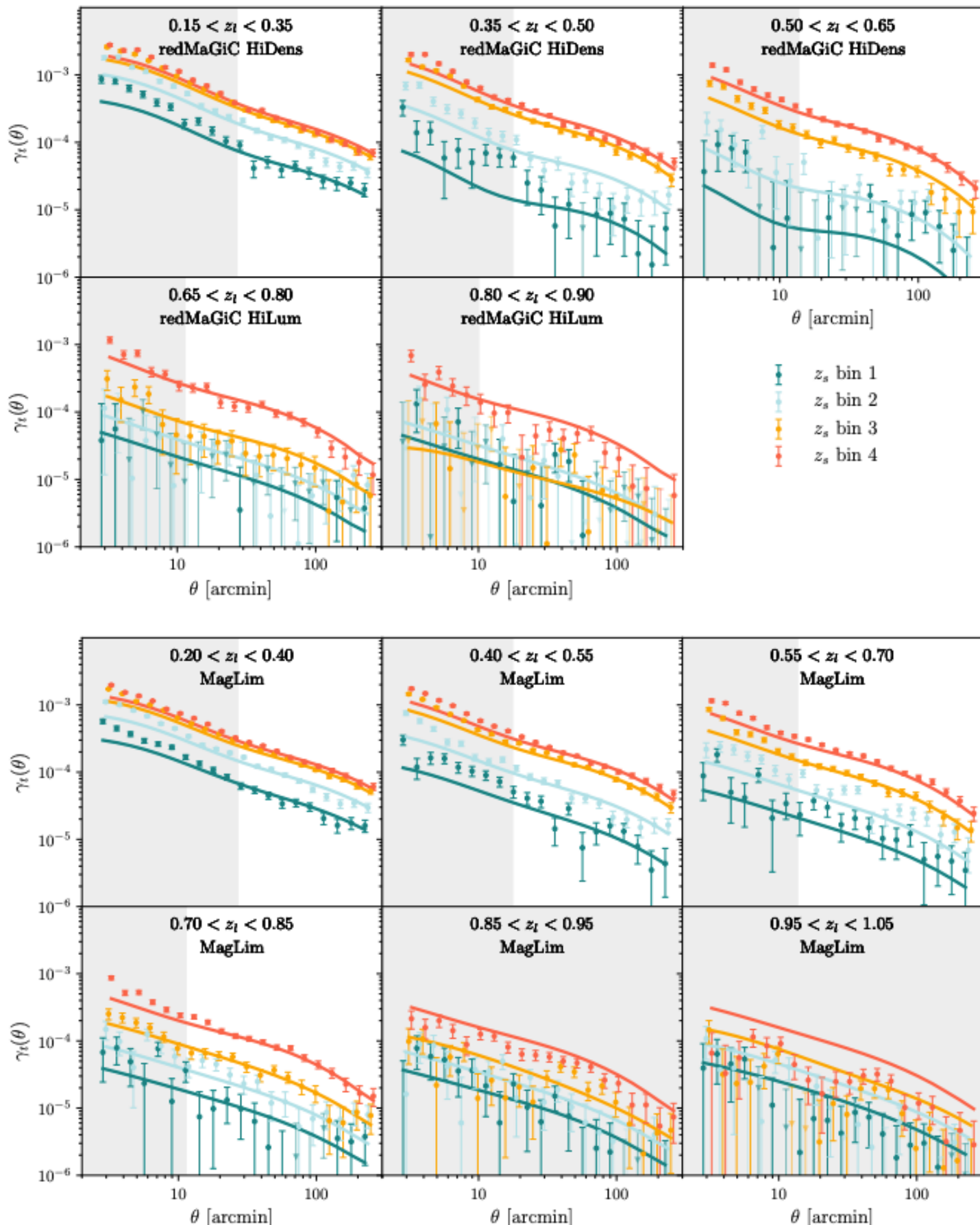


*Velander, et al. 2021*

# GALAXY-GALAXY LENSING

*DES - Dark Energy Survey*

*average tangential shear as a functions of angular distance from lens galaxy for different lens redshifts and lens galaxy populations*



# GALAXY-GALAXY LENSING

*Lee et al. (2022) DES-CMASS*

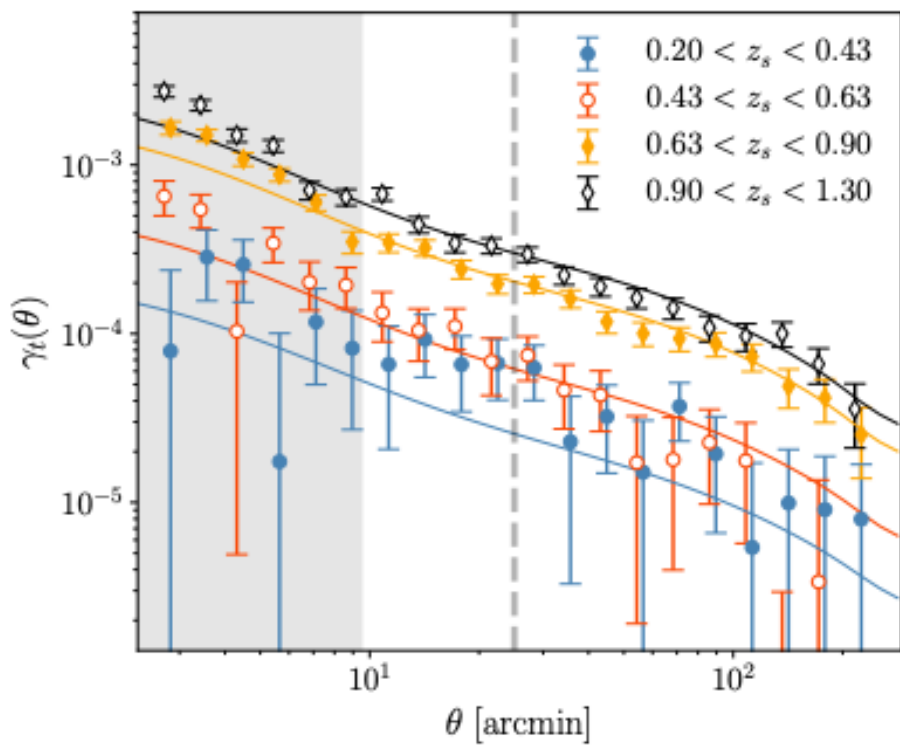
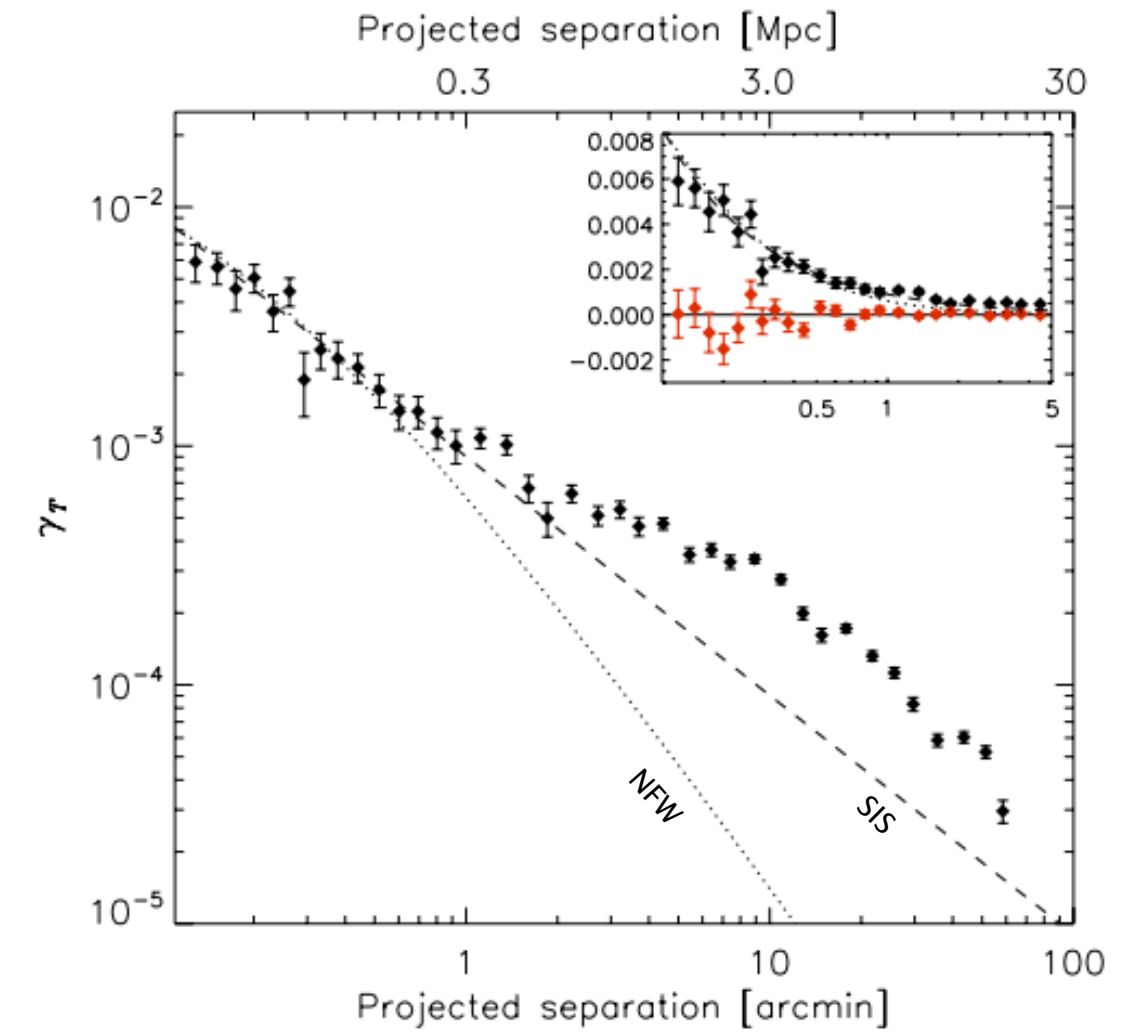


**Figure 6.** Tangential shear signals measured with the DMASS lenses and METACALIBRATION sources. The solid lines are the best-fit theory lines. The shaded region is the scales removed by the  $4h^{-1}$  Mpc scale cut. The vertical dashed line indicates the scale cut of  $12h^{-1}$  Mpc.



*van Uitert, et al. 2011*

$$\Delta\Sigma(R) \simeq \frac{1}{N\Sigma(\bar{z}_l, \bar{z}_s)} \sum_{R-\delta < |x_i - y_j| D_s < R+\delta} \epsilon_t^i \Sigma_{\text{crit}}(z_i, z_j)$$

*In addition the shear can be weighted to maximise signal-to-noise.*

# COSMOLOGICAL DISTANCES

---

coordinate distance

$$\chi(z_s) = \frac{c}{H_o} \int_0^{z_s} \frac{dz}{\sqrt{\Omega_m(1+z)^3 + \Omega_\Lambda + (1-\Omega_m-\Omega_\Lambda)(1+z)^2}}$$

critical density

$$\Omega_m = \frac{\rho}{\rho_{\text{crit}}} \quad \rho_{\text{crit}} = \frac{3H_o^2}{8\pi G} \quad H_o \quad \text{Hubble parameter}$$

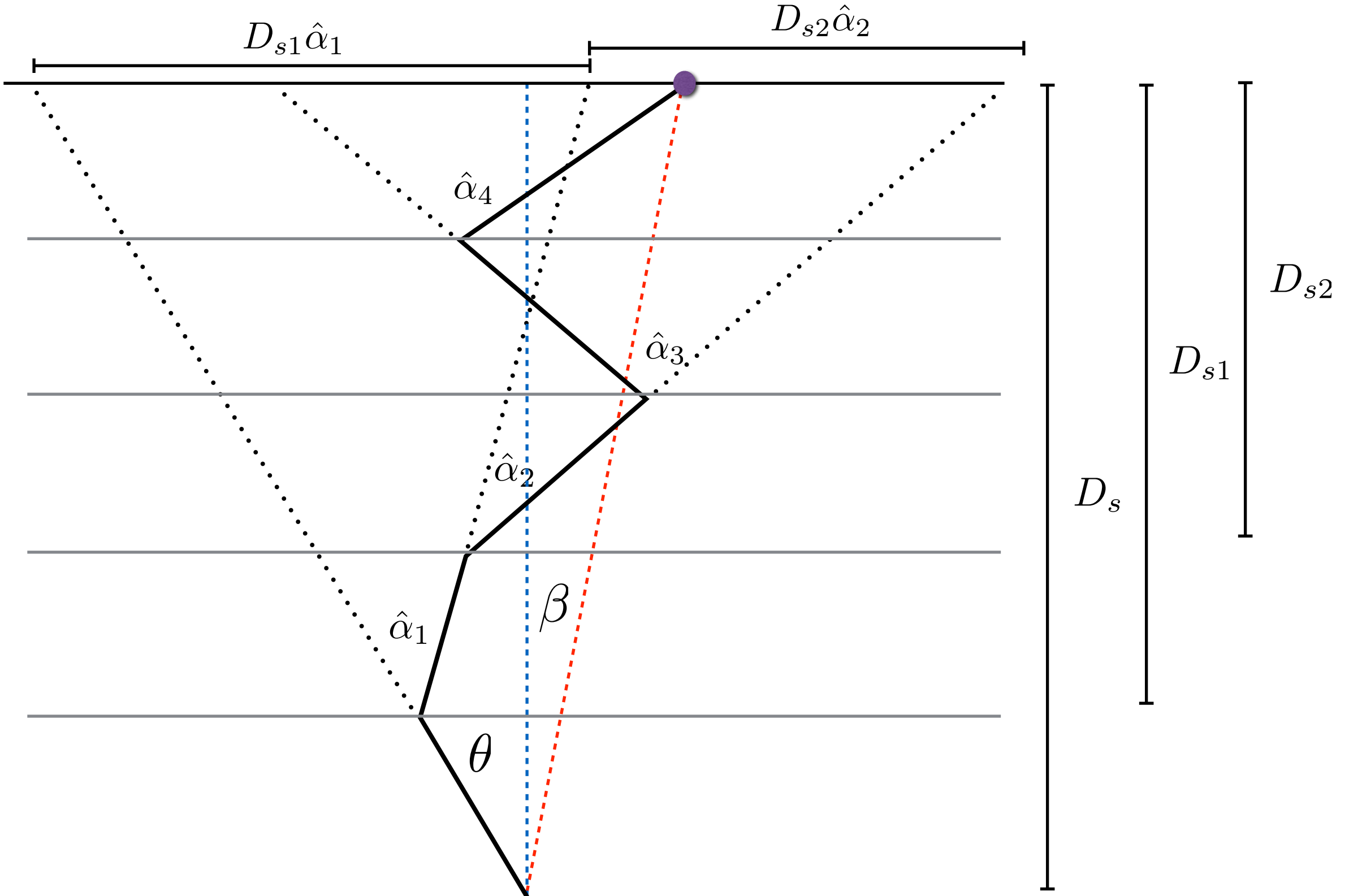
curvature distance

comoving angular size distance

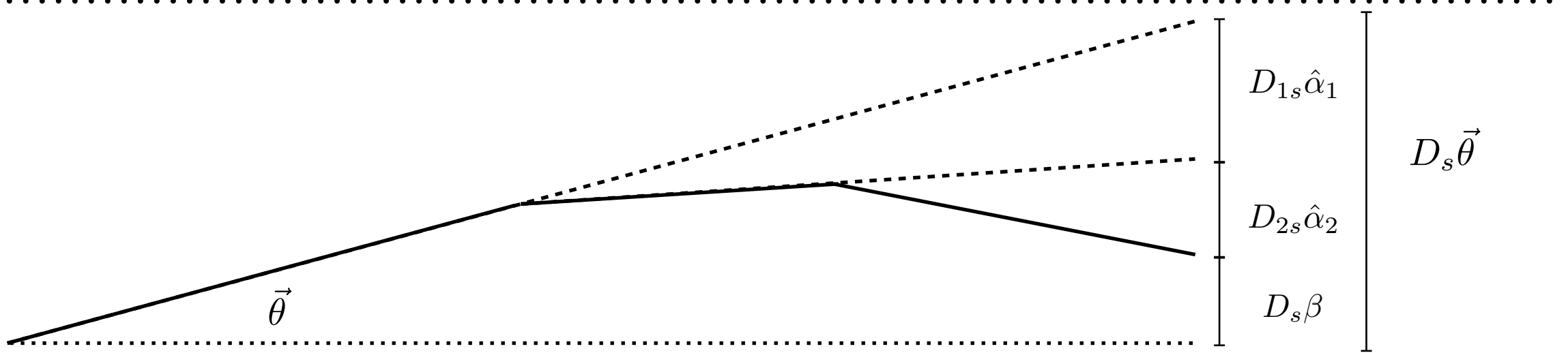
$$R_{\text{curv}} = \frac{c}{H_o \sqrt{1 - \Omega_m - \Omega_\Lambda}}$$

$$(1+z_2)D(z_1, z_2) = D_{CA}(z_1, z_2) = f(\chi_1 - \chi_2) = \begin{cases} R_{\text{curv}} \sin \left( \frac{\chi_1 - \chi_2}{R_{\text{curv}}} \right) & \Omega_m + \Omega_\Lambda < 1 \\ \chi_1 - \chi_2 & \Omega_m + \Omega_\Lambda = 1 \\ R_{\text{curv}} \sinh \left( \frac{\chi_1 - \chi_2}{R_{\text{curv}}} \right) & \Omega_m + \Omega_\Lambda > 1 \end{cases}$$

$$D_s \vec{\beta} = D_s \vec{\theta} - \sum_i D_{si} \hat{\alpha}_i (\vec{x}_i)$$



# THE CONTINUUM LIMIT



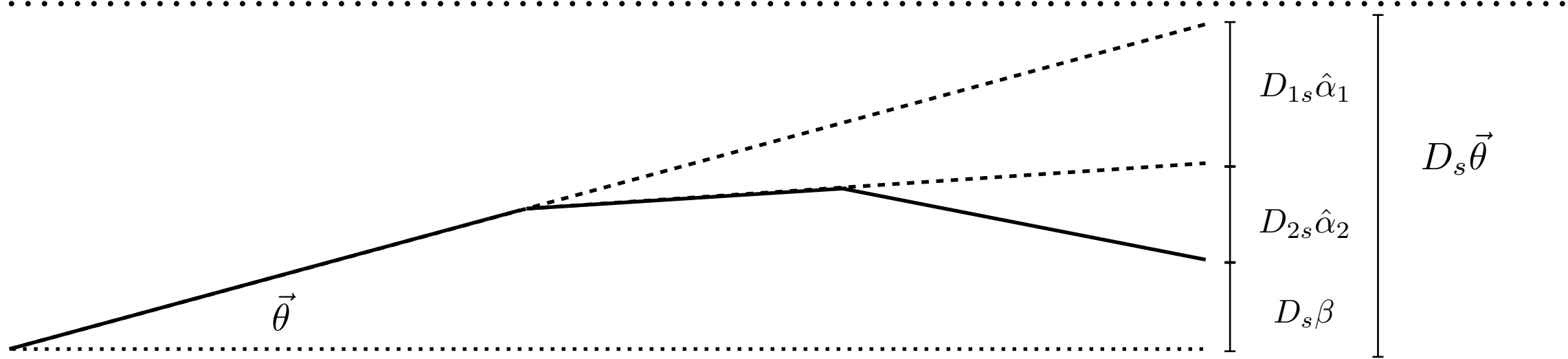
$$\beta = \theta - \frac{1}{D_s} \sum D_{si} \hat{\alpha}(\mathbf{x}_\perp)$$

$$\beta = \theta - \frac{2}{D_s c^2} \sum_i D_{si} \delta \chi \nabla_\perp \phi(\mathbf{x}_\perp, \chi_i) \quad \hat{\alpha}_i = \delta \chi \frac{2}{c^2} \nabla \phi$$

$$\beta = \theta - \frac{2}{D_s c^2} \int_0^\chi d\chi' D_{si} \nabla_\perp \phi(\mathbf{x}_\perp, \chi')$$

$$\beta = \theta - \frac{2}{c^2} \int_0^\chi d\chi' \frac{f(\chi - \chi')}{f(\chi)} \nabla_\perp \phi(\mathbf{x}_\perp, \chi')$$

# THE CONTINUUM LIMIT

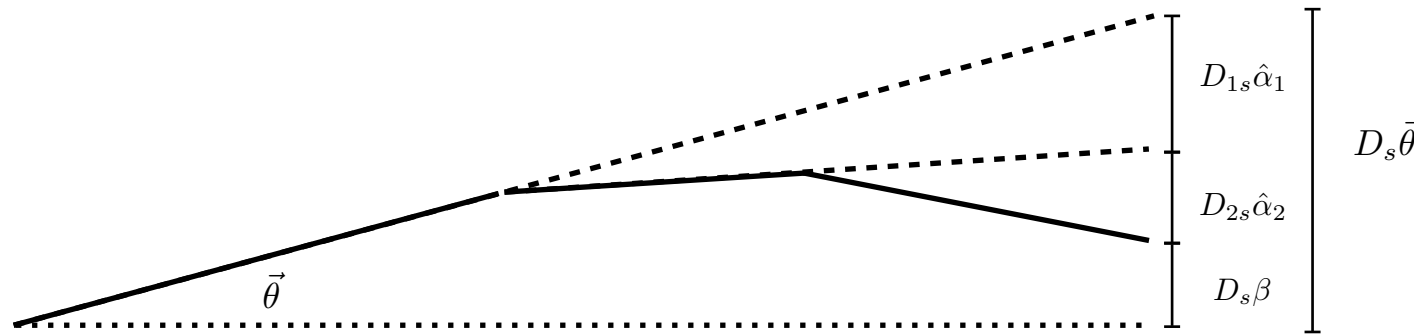


$$\beta = \theta - \frac{2}{c^2} \int_0^\chi d\chi' \frac{f(\chi - \chi')}{f(\chi)} \nabla_\perp \phi(\mathbf{x}_\perp, \chi')$$

Taking the derivative we get the magnification matrix :

$$\frac{\partial \beta_i}{\partial \theta_j} = \delta_{ij} - \frac{2}{c^2} \int_0^\chi d\chi' \frac{f(\chi - \chi')}{f(\chi)} \sum_k \left[ \frac{\partial x_k}{\partial \theta_j} \right] \frac{\partial \phi(\mathbf{x}_\perp, \chi')}{\partial x_i \partial x_k}$$

# BORN APPROXIMATION



The Born approximation is where the light path is taken to be that of an unperturbed ray and the deflection is a sum of the deflections without coupling between them.

$$\boldsymbol{x}_\perp = \boldsymbol{\theta} f(\chi)$$

$$\left[ \frac{\partial x_k}{\partial \theta_j} \right] = f(\chi) \delta_{kj}$$

$$\frac{\partial \beta_i}{\partial \theta_j} = \delta_{ij} - \frac{2}{c^2} \int_0^\chi d\chi' \left[ \frac{f(\chi - \chi') f(\chi')}{f(\chi)} \right] \frac{\partial \phi(\boldsymbol{\theta} f(\chi'), \chi')}{\partial x_i \partial x_k}$$

$$\kappa(\boldsymbol{\theta}) = 1 - \frac{1}{2} \text{tr} \left[ \frac{\partial \beta_i}{\partial \theta_j} \right] = \frac{3H_o^2 \Omega_m}{2c^2} \int_0^\chi d\chi' \left[ \frac{f(\chi - \chi') f(\chi')}{a(\chi') f(\chi)} \right] \delta(\boldsymbol{\theta} f(\chi'), \chi')$$

# CORRELATION FUNCTIONS AND POWER SPECTRA

---

Like other qualities, the convergence and shear are related to the 3D density distribution in this way.

$$h_i(\boldsymbol{\theta}) = \int_0^{\chi_s} d\chi \ w_1(\chi) \ \delta(f(\chi)\boldsymbol{\theta}, \chi)$$

$$\begin{aligned}\xi_{ij}(\phi) &= \langle h_i(\boldsymbol{\theta}) h_j(\boldsymbol{\theta}') \rangle & \phi &= \boldsymbol{\theta} - \boldsymbol{\theta}' \\ &= \int_0^{\chi_s} d\chi \ w_1(\chi) \int_0^{\chi_s} d\chi' \ w_2(\chi') \xi_\delta(s) & s^2 &= (\chi - \chi')^2 + (f(\chi)\boldsymbol{\theta} - f(\chi')\boldsymbol{\theta}')^2\end{aligned}$$

Beyond some distance,  $s$ , the correlation function will be very small.

Changing to coordinates     $\bar{\chi} = (\chi + \chi')/2$      $\Delta_\chi = \chi - \chi'$

If the window functions    are approximately constant over this range, they can  
Limber's equation

$$\xi_{ij}(\phi) \simeq \int_0^{\chi_s} d\chi \ w_1(\chi) w_2(\chi) \int d\Delta_\chi \ \xi_\delta \left( \sqrt{f(\chi)|\boldsymbol{\phi}|^2 + \Delta_\chi^2}, \chi \right)$$

# CORRELATION FUNCTIONS AND POWER SPECTRA

---

$$\xi_{ij}(\phi) \simeq \int_0^{\chi_s} d\chi \ w_1(\chi)w_2(\chi) \int d\Delta_\chi \ \xi_\delta \left( \sqrt{f(\chi)|\phi|^2 + \Delta_\chi^2}, \chi \right) \quad \textit{Limber's equation}$$

$$\xi_{ij}(\phi) \simeq \int_0^{\chi_s} d\chi \ w_1(\chi)w_2(\chi) \int \frac{d^3k}{(2\pi)^3} P_\delta(\mathbf{k}_\perp, k_\parallel) \int d\Delta_\chi \ \exp(-if(\chi) \cdot \mathbf{k}_\perp - i\Delta_\chi k_\parallel)$$

$$= \int_0^{\chi_s} d\chi \ w_1(\chi)w_2(\chi) \int \frac{d^2k_\perp}{(2\pi)^2} P_\delta(\mathbf{k}_\perp, 0) \exp(-if(\chi) \phi \cdot \mathbf{k}_\perp)$$

# CORRELATION FUNCTIONS AND POWER SPECTRA

---

$$h_i(\boldsymbol{\theta}) = \int_0^{\chi_s} d\chi \ w_1(\chi) \ \delta(f(\chi)\boldsymbol{\theta}, \chi)$$

$$\xi_{ij}(\phi) \simeq \int_0^{\chi_s} d\chi \ w_1(\chi) w_2(\chi) \int \frac{d^3k}{(2\pi)^3} P_\delta(\mathbf{k}_\perp, k_\parallel) \int d\Delta_\chi \ \exp(-if(\chi) \cdot \mathbf{k}_\perp - i\Delta_\chi k_\parallel)$$

$$= \int_0^{\chi_s} d\chi \ w_1(\chi) w_2(\chi) \int \frac{d^2k_\perp}{(2\pi)^2} P_\delta(\mathbf{k}_\perp, 0) \exp(-if(\chi) \boldsymbol{\phi} \cdot \mathbf{k}_\perp)$$

$$P(\boldsymbol{\ell}) = \int d^2\phi \ e^{i\boldsymbol{\ell}\cdot\boldsymbol{\phi}} \xi_{ij}(\phi)$$

$$= \int_0^{\chi_s} d\chi \ w_1(\chi) w_2(\chi) \int \frac{d^2k_\perp}{(2\pi)^2} P_\delta(\mathbf{k}_\perp, 0) \int d^2\phi \ \exp[-i(f(\chi) \boldsymbol{\phi} \cdot \mathbf{k}_\perp - \boldsymbol{\ell} \cdot \boldsymbol{\phi})]$$

$$= \int_0^{\chi_s} d\chi \ w_1(\chi) w_2(\chi) \int \frac{d^2k_\perp}{(2\pi)^2} P_\delta(\mathbf{k}_\perp, 0) (2\pi)^2 \delta^D(f(\chi) \mathbf{k}_\perp - \boldsymbol{\ell})$$

$$= \int_0^{\chi_s} d\chi \ \frac{w_1(\chi) w_2(\chi)}{f(\chi)^2} P_\delta\left(\frac{\boldsymbol{\ell}}{f(\chi)}\right) \quad \textit{Fourier space Limber's equation}$$

# WEAK LENSING : E & B MODES

---

*In general a vector field in two dimensions can be decomposed into the gradient of a potential (the electric or E-field) and a pseudo-scalar or curl field (magnetic or B-field).*

$$\alpha_i = \partial_i \phi^E + \epsilon_{ij} \partial_j \phi^B$$

*or*

$$\alpha_1 = \partial_1 \phi^E + \partial_2 \phi^B$$

$$\alpha_2 = \partial_2 \phi^E - \partial_1 \phi^B$$

*We now have two potentials, but only the E-field can be generated by weak lensing*

# WEAK LENSING : E & B MODES

---

*In general a vector field in two dimensions can be decomposed into the gradient of a potential (the electric or E-field) and a pseudo-scalar or curl field (magnetic or B-field).*

$$\alpha_i = \partial_i \phi^E + \epsilon_{ij} \partial_j \phi^B$$

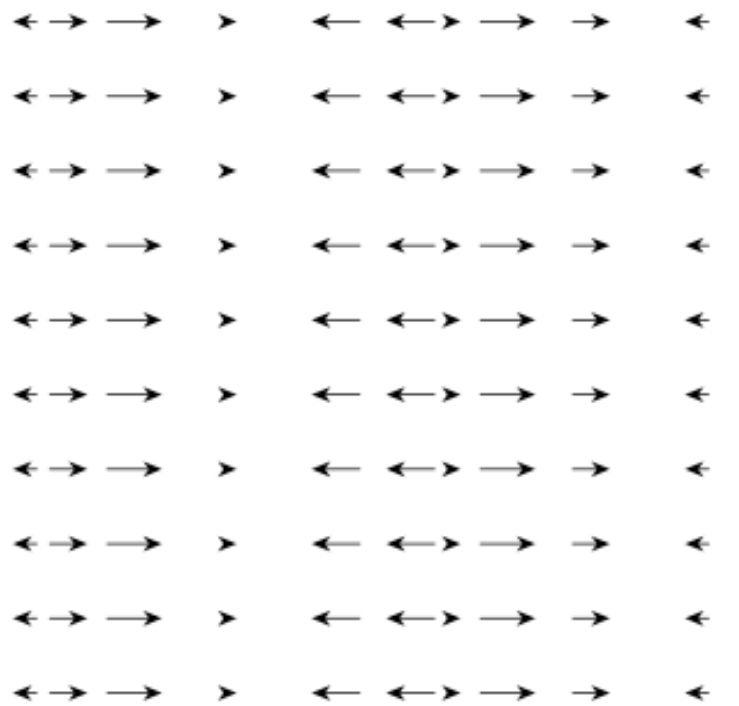
*The appropriate shear matrix (the one that would be estimated by the ellipticity of galaxies in the weak shear limit) is given by*

$$\gamma_{ij} = (\partial_i \partial_j - \frac{1}{2} \nabla^2) \phi^E + \frac{1}{2} (\epsilon_{kj} \partial_k \partial_i + \epsilon_{ki} \partial_k \partial_j) \phi^B$$

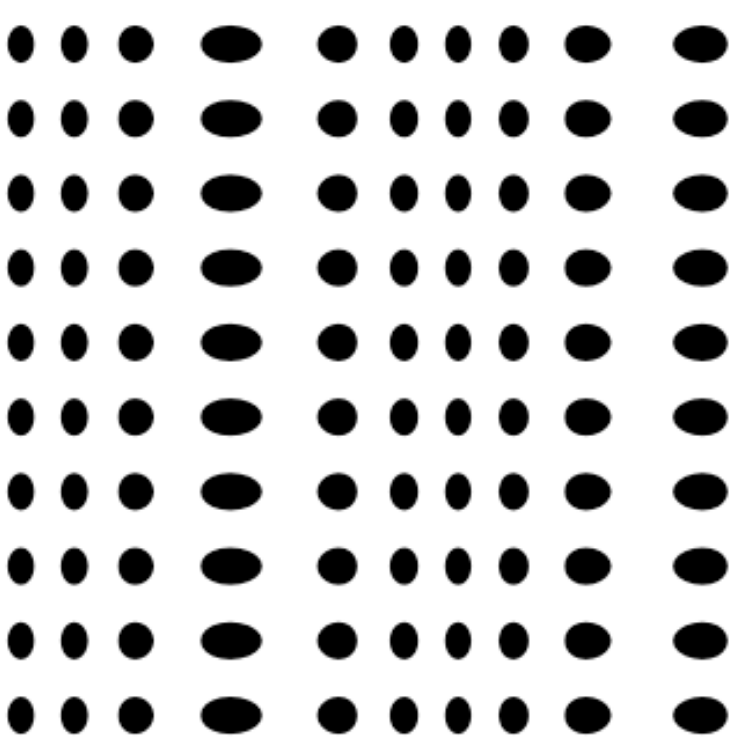
# WEAK LENSING : E & B MODES

---

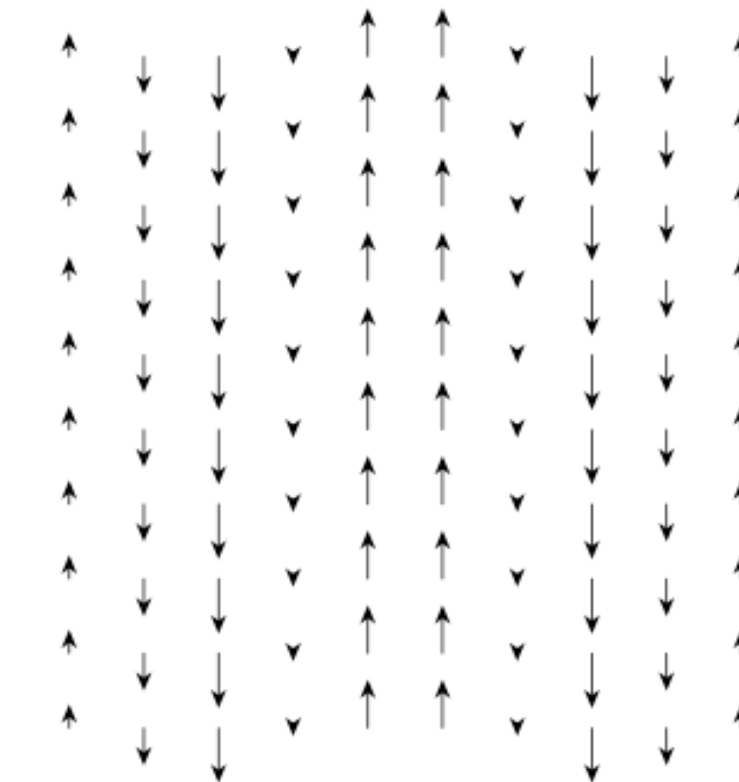
*E-mode or  
scalar field  
deflection pattern*



*E-mode or  
scalar field  
ellipticity pattern*



*B-mode or  
pseudo scalar field  
deflection pattern*



*B-mode or  
pseudo scalar field  
ellipticity pattern*

# WEAK LENSING : E & B MODES

---

*E and B mode decomposition*

$$\kappa = \frac{1}{2} \nabla^2 \phi^E \quad \kappa^B = \frac{1}{2} \nabla^2 \phi^B$$

*Using the previous formula it can be shown that*

$$\nabla^2 \kappa = \partial_i \partial_j \gamma_{ij} = (\partial_1^2 - \partial_2^2) \gamma_1 + 2\partial_1 \partial_2 \gamma_2$$

$$\nabla^2 \kappa^B = \epsilon_{ij} \partial_i \partial_k \gamma_{jk} = (\partial_1^2 - \partial_2^2) \gamma_2 - 2\partial_1 \partial_2 \gamma_1$$

*The first formula can be used to reconstruct the convergence with the usual Kaiser & Squires method or an equivalent.*

*The second can be used to reconstruct the B-mode which should be close to zero.*

*Note that this is equivalent to rotating each galaxy by  $45^\circ$  and then reconstructing  $\kappa$ .*

# WEAK LENSING : E & B MODES

---

*The B modes add noise to the lensing measurements and so generally need to be filtered out using statistics that are only sensitive to the E modes.*

*In a finite field the decomposition into E and B fields is not unique.*

***contributions to the B-modes:***

*Multi-plane lensing effects. These are second order in the shear and convergence and thus are generally small.*

*Intrinsic correlations between galaxy shapes.*

*Higher order terms in the relation between galaxy ellipticity and shear.*

*Image and data analysis error such as PSF correction residuals, systematics in astrometry, etc.*

*Exotic things like vector and tensor perturbations which are expected to be very small.*

# LINEAR STRUCTURE FORMATION

---

Fluid equations

$$\frac{\partial \rho}{\partial t} + \nabla_r \cdot (\rho \vec{u}) = 0 \quad \text{mass conservation}$$

$$\frac{\partial \vec{u}}{\partial t} + (\vec{u} \cdot \nabla_r) \vec{u} = -\nabla_r \Phi_N \quad \text{Euler's equation}$$

$$\nabla_r^2 \Phi_N = 4\pi G \rho \quad \text{Poisson's equation}$$

Change of variables

$$\delta = \frac{\rho - \bar{\rho}}{\bar{\rho}} \quad \text{mass} \qquad \vec{x} = \frac{\vec{r}}{a(t)} \quad \text{comoving coordinates}$$

$$\phi = \Phi_N - \frac{2}{3}\pi G \rho r^2 + \frac{1}{6}\Lambda r^2$$

Combining these and dropping all terms nonlinear in  $\rho$  gives

$$\frac{\partial^2 \delta}{\partial t^2} + 2 \left( \frac{\dot{a}}{a} \right) \frac{\partial \delta}{\partial t} = 4\pi G \bar{\rho} \delta$$

# LINEAR STRUCTURE FORMATION

---

$$\frac{\partial^2 \delta}{\partial t^2} + 2 \left( \frac{\dot{a}}{a} \right) \frac{\partial \delta}{\partial t} = 4\pi G \bar{\rho} \delta$$

or with Friedmann's equation

$$\frac{\partial^2 \delta}{\partial t^2} + 2H_o \left[ \frac{\rho_{\text{background}}(t)}{\rho_{\text{crit}}} \right]^{1/2} \frac{\partial \delta}{\partial t} = 4\pi G \bar{\rho} \delta$$

this admits a linear solution

$$\delta(\vec{x}, t) = D(t) \delta(\vec{x}, t = t_o)$$

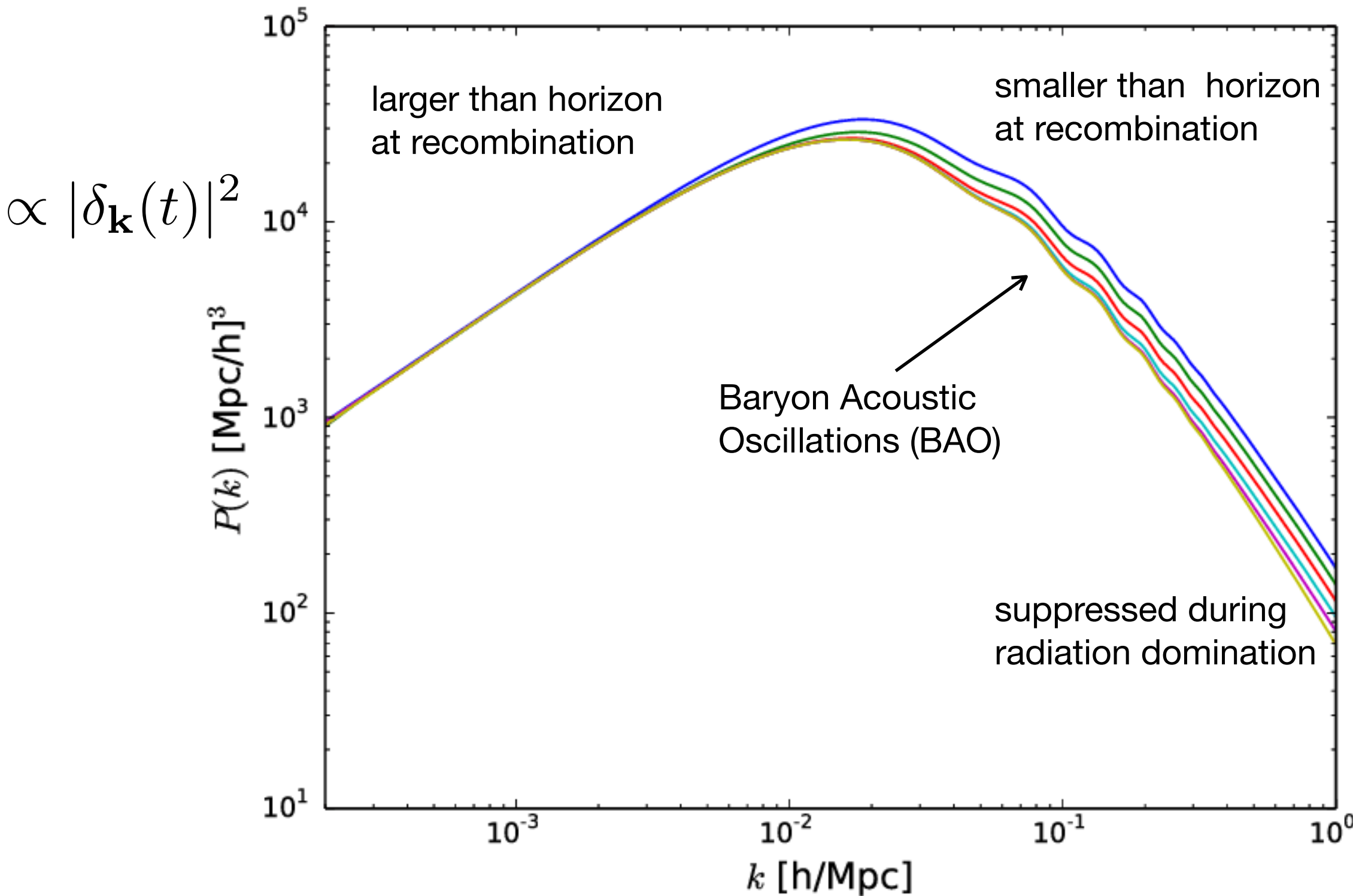
*The power spectrum will scale like:*

$$P_\delta(k, t) = D(t)^2 P_\delta(k, t = t_o)$$

# LINEAR STRUCTURE FORMATION

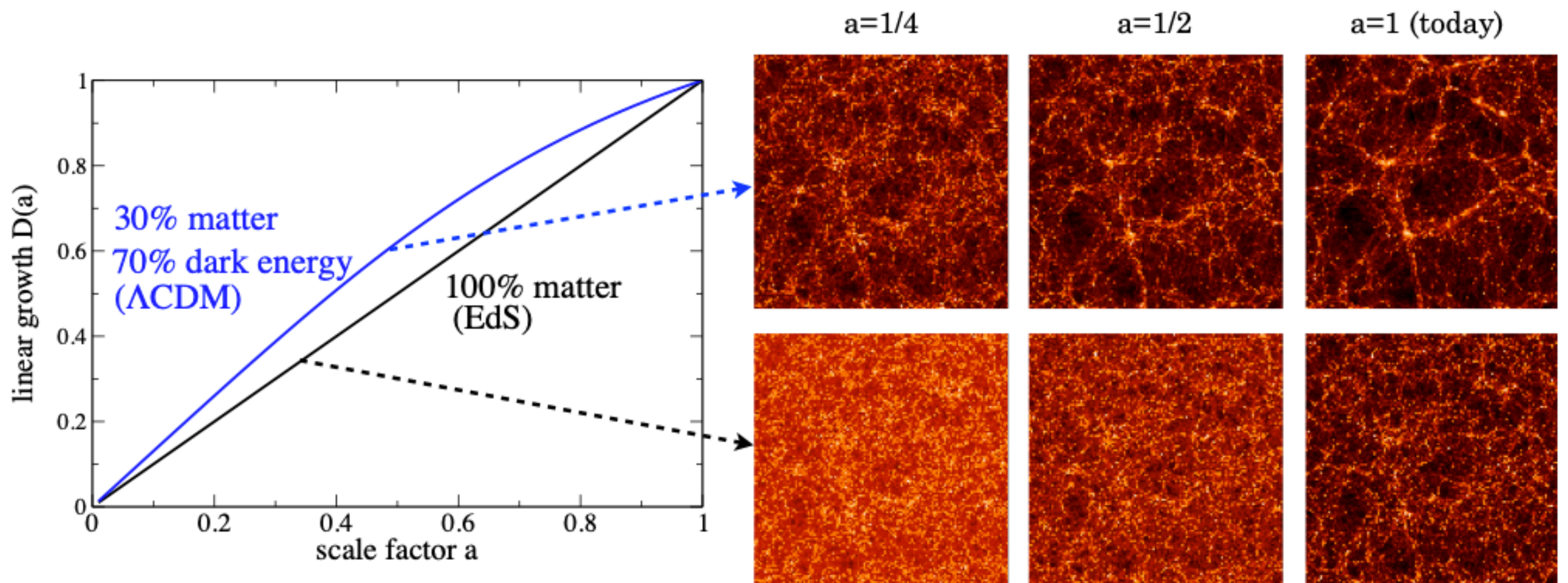
---

*Matter power spectrum from the distribution of galaxies*



# LINEAR STRUCTURE FORMATION

---



# APERTURE MASS STATISTIC

---

*The aperture mass statistic is an axially symmetric filtering of the tangential shear.*

$$\begin{aligned} M_{ap}(\theta, R) &= \int d^2\theta' \gamma_t(\theta') Q_R(|\theta' - \theta|) \\ &= \int d^2\theta' \kappa(\theta') U_R(|\theta' - \theta|) \end{aligned}$$

*where*  $\int d^2\theta U_R(\theta) = 0$  *filters out mass sheet*

*By requiring the equality above it can be easily shown that the window functions must be related by*

$$U(\theta) = 2 \int_0^\theta d\theta' \frac{Q(\theta')}{\theta'} - Q(\theta) \quad Q(\theta) = \frac{2}{\theta^2} \int_0^\theta d\theta' \theta' U(\theta') - U(\theta)$$

*A convenient function  $U(\theta)$  or  $Q(\theta)$  can be chosen and the other found from these relations.*

*If  $\gamma_t$  is used this will only be dependent on the B-modes. Substituting  $\gamma_x$  will make it B-mode only which can be used as a check on systematics.*

# CORRELATION FUNCTIONS AND POWER SPECTRA

---

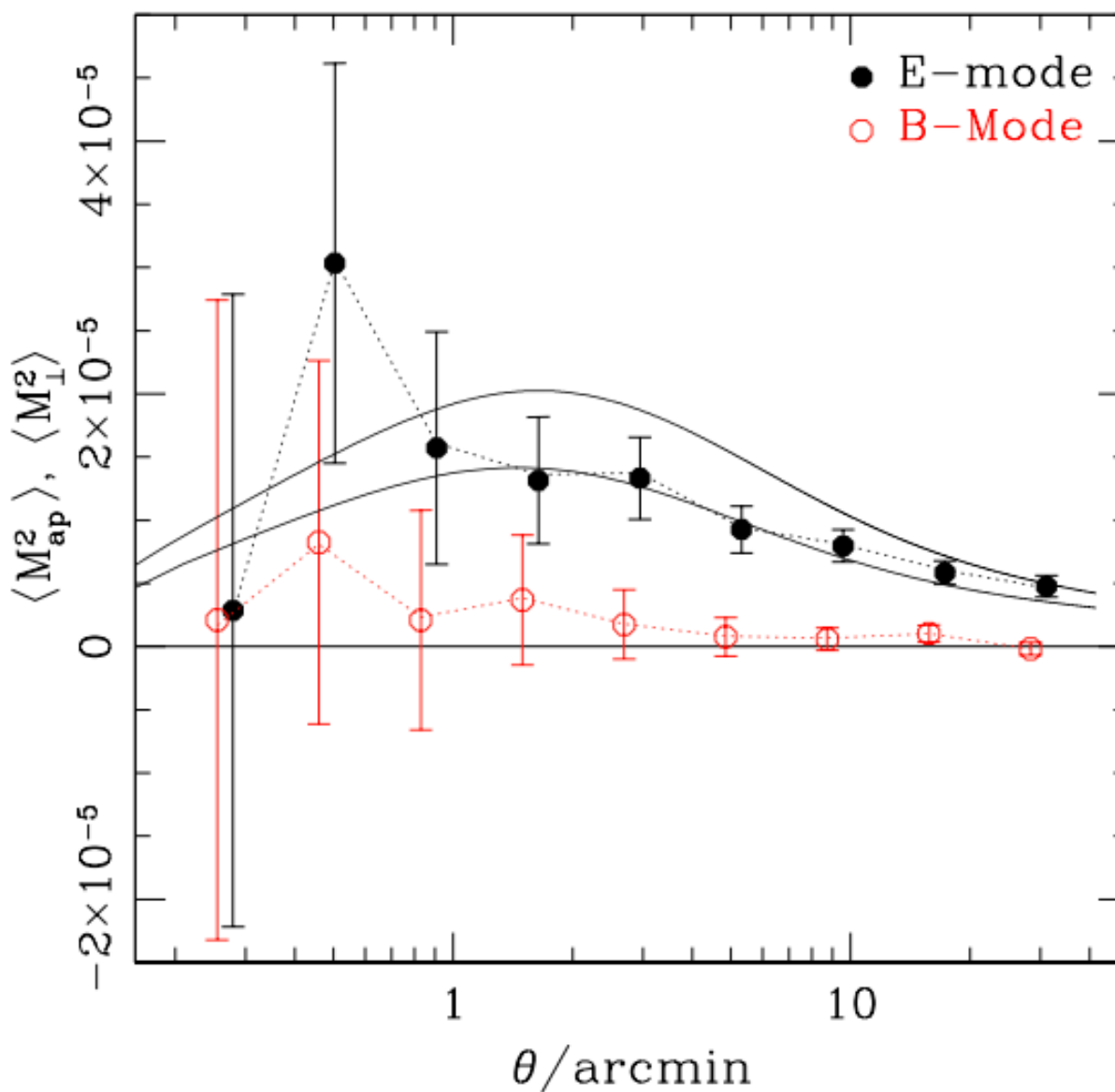


**Figure 5.** Aperture-mass dispersion measured in COSMOS. The two solid lines correspond to predictions with  $\sigma_8 = 0.7$  and  $0.8$ , respectively. From Schrabback et al. (2010). Figure reproduced with permission from Schrabback et al. (2010), *A&A*, **516**, A63. © ESO.



# CORRELATION FUNCTIONS AND POWER SPECTRA

---

*Shear correlation functions can be constructed. It is traditional to define :*

$$\begin{aligned}\xi_+ &= \xi_{\parallel} + \xi_{\angle} = \langle \gamma_1^{(i)} \gamma_1^{(j)} \rangle + \langle \gamma_2^{(i)} \gamma_2^{(j)} \rangle \\ \xi_- &= \xi_{\parallel} - \xi_{\angle} = [\langle \gamma_1^{(i)} \gamma_1^{(j)} \rangle - \langle \gamma_2^{(i)} \gamma_2^{(j)} \rangle] \cos(4\phi_{ij})\end{aligned}$$

$$\langle \gamma_1^{(i)} \gamma_2^{(j)} \rangle = 0$$

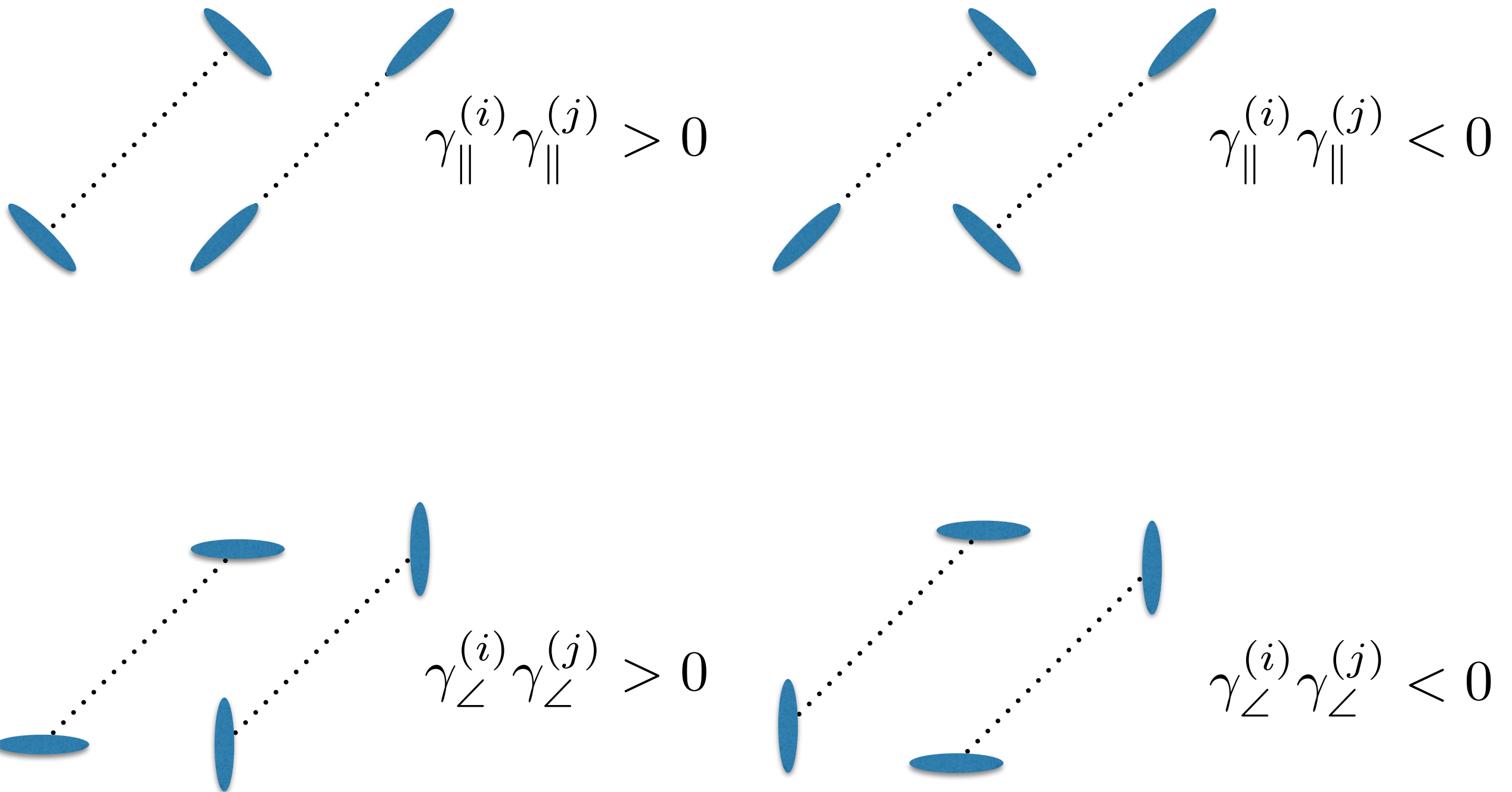
*An estimator for the correlation functions is*

$$\hat{\xi}_{\pm} = \frac{\sum_{ij} w_i w_j [\epsilon_{\parallel}^{(i)} \epsilon_{\parallel}^{(j)} \pm \epsilon_{\angle}^{(i)} \epsilon_{\angle}^{(j)}]}{\sum_{ij} w_i w_j}$$

*where the sum is over all pairs within a bin in angular separation. The w's are weights that can be adjusted to down weight high noise measurement relative to low noise measurements.*

# *Observing Cosmic Shear*

## *Shear Correlation Function*



# CORRELATION FUNCTIONS AND POWER SPECTRA

---

$$\xi_+ = \xi_{\parallel} + \xi_{\angle} = \langle \gamma_1^{(i)} \gamma_1^{(j)} \rangle + \langle \gamma_2^{(i)} \gamma_2^{(j)} \rangle$$
$$\xi_- = \xi_{\parallel} - \xi_{\angle} = [\langle \gamma_1^{(i)} \gamma_1^{(j)} \rangle - \langle \gamma_2^{(i)} \gamma_2^{(j)} \rangle] \cos(4\phi_{ij})$$

*These correlation functions have contributions from both the E-modes and B-modes. In terms of the power spectra of the two convergences these can be written.*

$$\xi_+(\theta) = \frac{1}{2\pi} \int d\ell \ell J_0(\ell\theta) [P_\kappa^E(\ell) + P_\kappa^B(\ell)]$$

$$\xi_-(\theta) = \frac{1}{2\pi} \int d\ell \ell J_4(\ell\theta) [P_\kappa^E(\ell) - P_\kappa^B(\ell)]$$

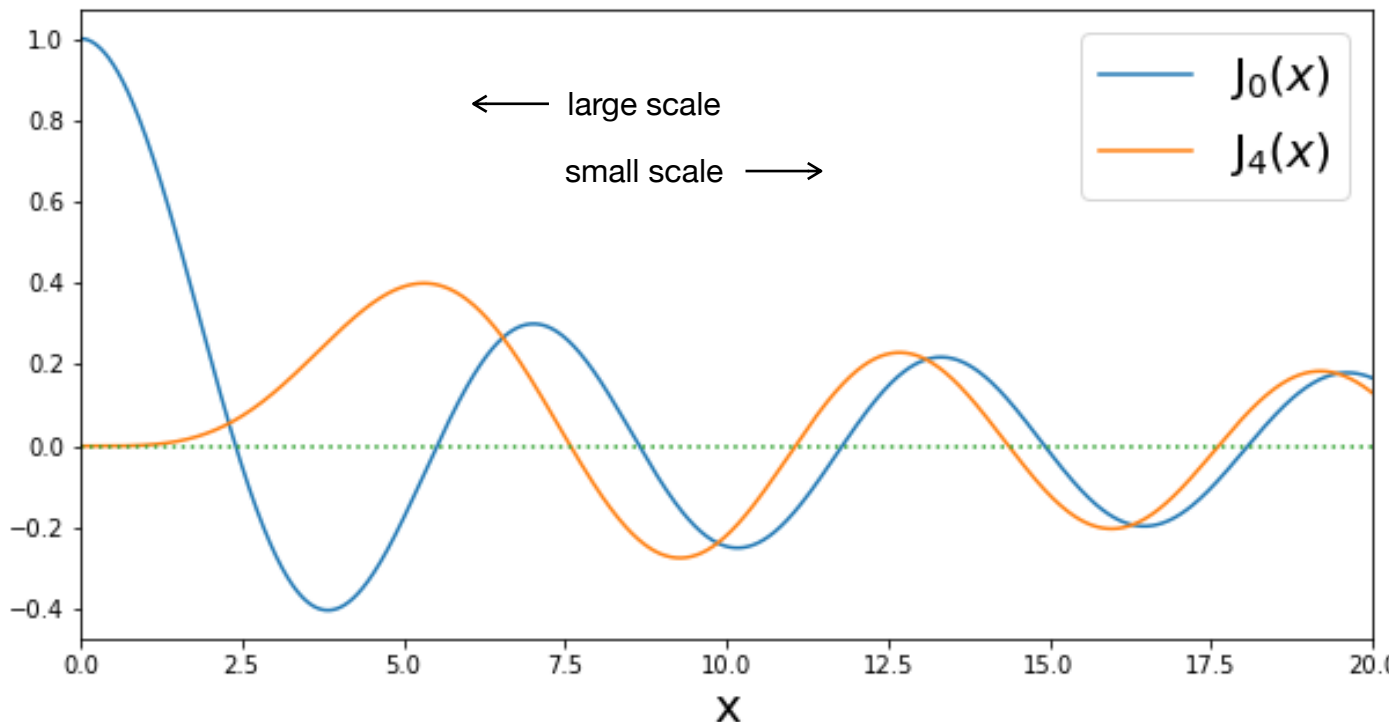
# CORRELATION FUNCTIONS AND POWER SPECTRA

---

$$\xi_+(\theta) = \frac{1}{2\pi} \int d\ell \ell J_0(\ell\theta) [P_\kappa^E(\ell) + P_\kappa^B(\ell)]$$

$$\xi_-(\theta) = \frac{1}{2\pi} \int d\ell \ell J_4(\ell\theta) [P_\kappa^E(\ell) - P_\kappa^B(\ell)]$$

Bessel functions



$\xi_-$  is more sensitive to smaller scales than  $\xi_+$

For this reason  $\xi_+$  is less sensitive to baryonic and nonlinear affects that are less accurately predicted by cosmological theory and simulation.

# CORRELATION FUNCTIONS AND POWER SPECTRA

---

$$\xi_+(\theta) = \frac{1}{2\pi} \int d\ell \ell J_0(\ell\theta) [P_\kappa^E(\ell) + P_\kappa^B(\ell)]$$

$$\xi_-(\theta) = \frac{1}{2\pi} \int d\ell \ell J_4(\ell\theta) [P_\kappa^E(\ell) - P_\kappa^B(\ell)]$$

*On the sphere these, correlation functions can be related to the power spectra in spherical harmonic space  $C_\kappa(\ell)$ .*

$$\xi_+(\theta) = \sum_{\ell} \frac{2\ell+1}{4\pi} G_\ell^\pm(\cos\theta) [C_{\kappa,\text{EE}}^{ij}(\ell) + C_{\kappa,\text{BB}}^{ij}(\ell)],$$

$$\xi_-(\theta) = \sum_{\ell} \frac{2\ell+1}{4\pi} G_\ell^\pm(\cos\theta) [C_{\kappa,\text{EE}}^{ij}(\ell) - C_{\kappa,\text{BB}}^{ij}(\ell)],$$

# CORRELATION FUNCTIONS AND POWER SPECTRA

---

$$\xi_+ = \xi_{\parallel} + \xi_{\angle} = \langle \gamma_1^{(i)} \gamma_1^{(j)} \rangle + \langle \gamma_2^{(i)} \gamma_2^{(j)} \rangle$$
$$\xi_- = \xi_{\parallel} - \xi_{\angle} = [\langle \gamma_1^{(i)} \gamma_1^{(j)} \rangle - \langle \gamma_2^{(i)} \gamma_2^{(j)} \rangle] \cos(4\phi_{ij})$$

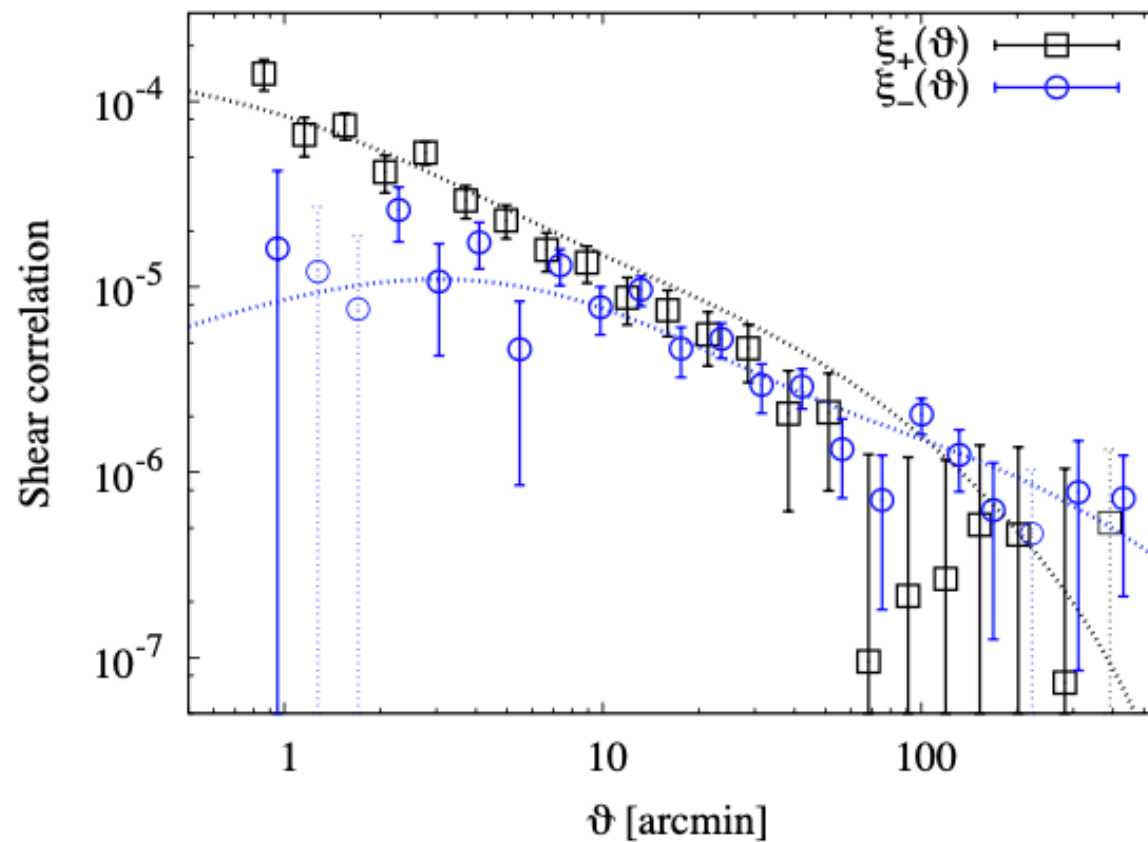


**Figure 4.** 2PCF components  $\xi_+$  and  $\xi_-$  (32) measured in CFHTLenS. The dotted lines show the WMAP7 model prediction (Komatsu et al. 2011). From Kilbinger et al. (2013). Copyright 2013 Oxford University Press.

# CORRELATION FUNCTIONS AND POWER SPECTRA

---

*These correlation functions have contributions from both the E-modes and B-modes.  
In terms of the power spectra of the two convergences these can be written.*

$$\xi_+(\theta) = \frac{1}{2\pi} \int d\ell \ell J_0(\ell\theta) [P_\kappa^E(\ell) + P_\kappa^B(\ell)]$$
$$\xi_-(\theta) = \frac{1}{2\pi} \int d\ell \ell J_4(\ell\theta) [P_\kappa^E(\ell) - P_\kappa^B(\ell)]$$

*(Semi-)Pure E-modes and B-modes statistics can be constructed from these correlation functions.*

*The statistics*

$$X_{E,B} = \frac{1}{2\pi} \int_0^\infty d\ell \ell P_\kappa^{E,B}(\ell) \tilde{w}(\ell)$$

*Can be estimated with*

$$\hat{X}_{E,B} = \frac{1}{2} \sum_i \theta_i \Delta\theta_i [T_+(\theta_i) \hat{\xi}_+(\theta_i) \pm T_-(\theta_i) \hat{\xi}_-(\theta_i)]$$

*where  $\Delta\theta_i$  is the bin width and*

$$T_{+,-}(\theta) = \int_0^\infty ds s J_{0,4}(s\theta) \tilde{w}(s)^2$$

*These are not actually pure E- and B-modes because there is typically "leakage" between them in finite and usually irregularly shaped field where data is available.*

*Pure modes can be constructed taking the survey geometry into account*

*Crittenden et al 2002  
Schneider & Kilbinger 2007*

# LENSING TOMOGRAPHY

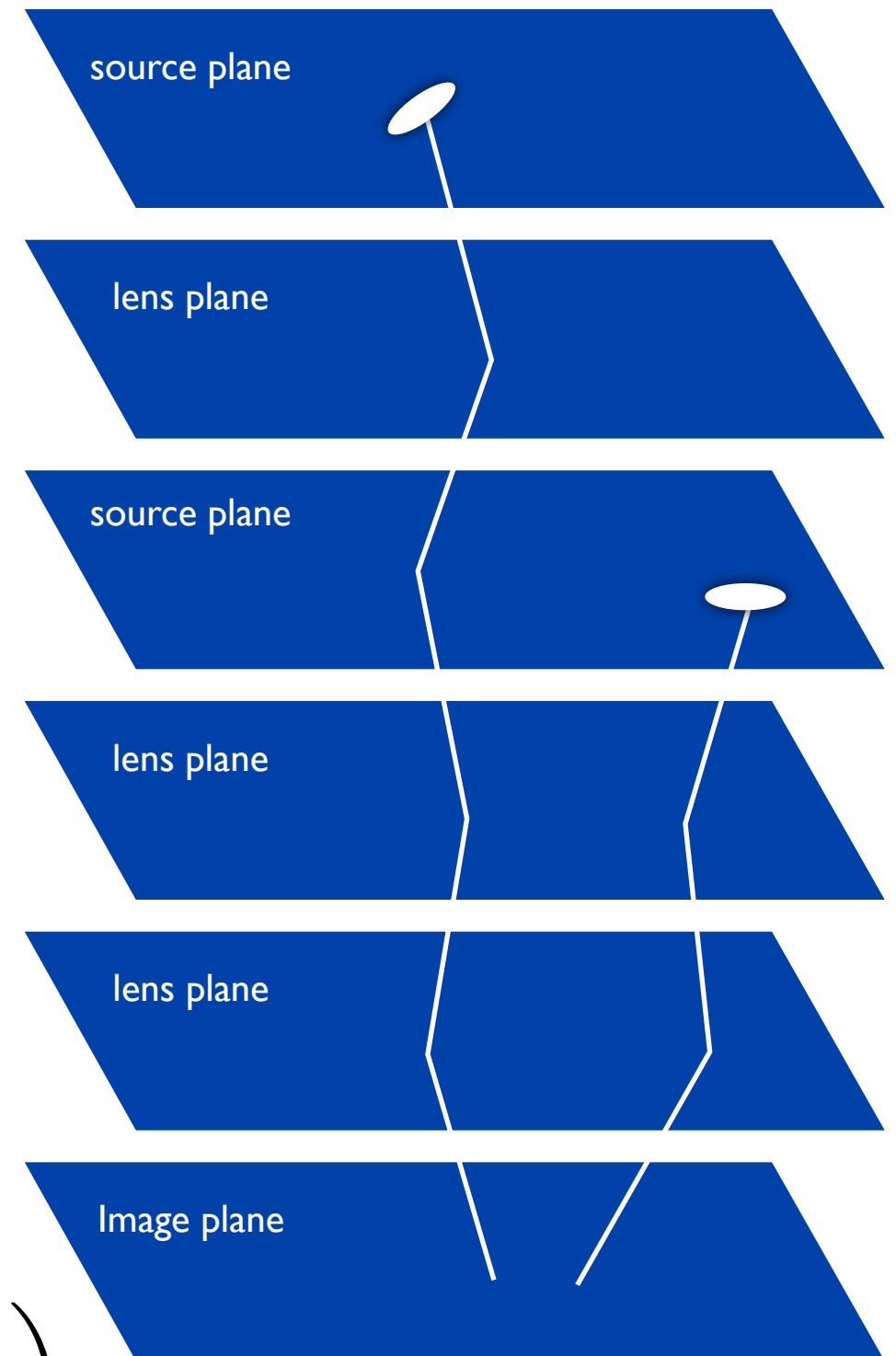
---

*Correlations between source redshift bins contain additional information about the evolution of structure formation and reduce systematics such as intrinsic galaxy alignments.*

*The shear signal can also be correlated with the foreground density of galaxies or other tracer of density. These can often be less noisy which increases the signal-to-noise, but at the expense of adding more parameters to describe the **bias** of the tracer relative to the density contrast.*

*Cross power spectrum between two observables.*

$$C_\ell^{12} = \int_0^{\chi_s} d\chi \frac{w_1(\chi)w_2(\chi)}{f(\chi)^2} P_\delta \left( \frac{\ell}{f(\chi)} \right)$$



# LENSING TOMOGRAPHY

---

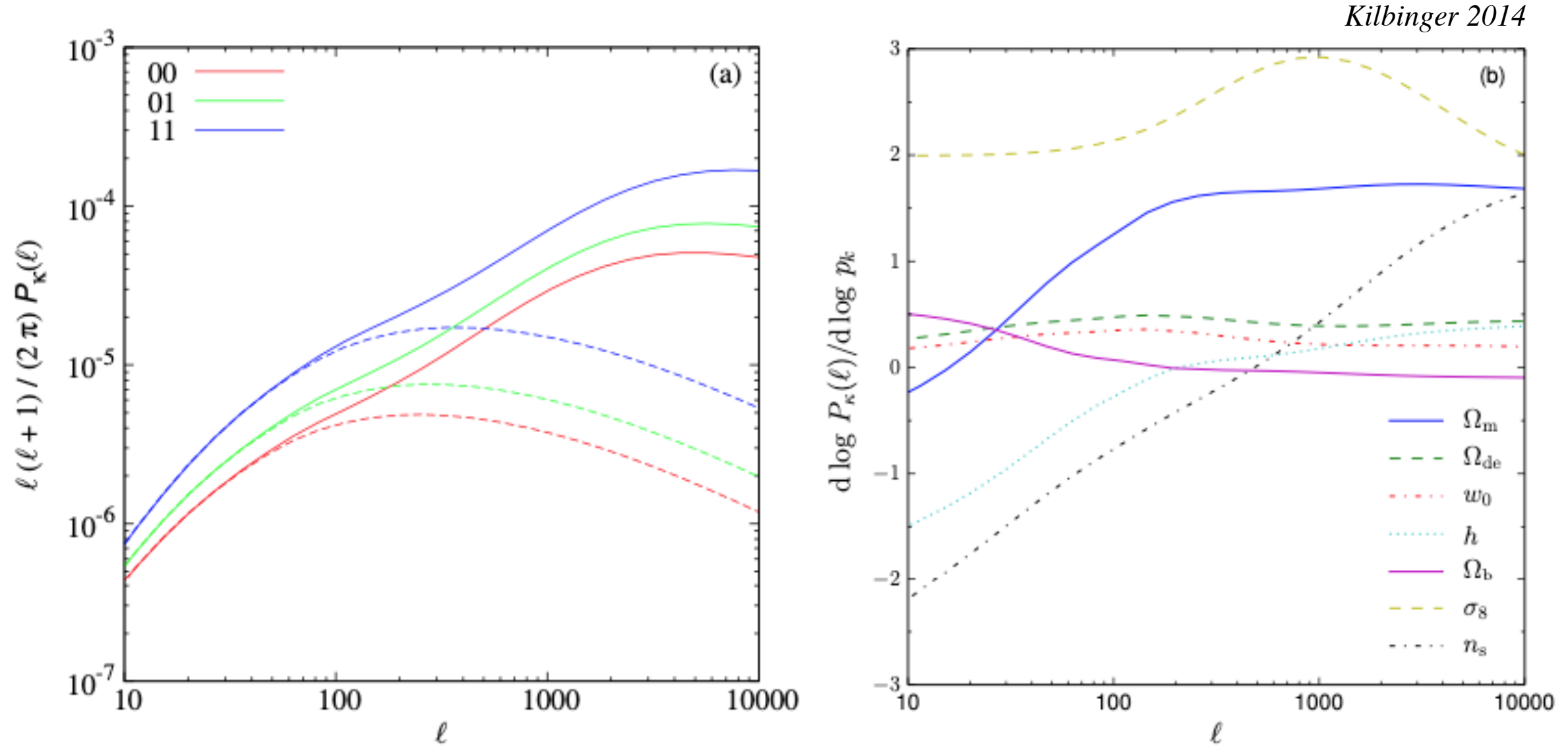


**Figure 3.** (a) The scaled tomographic convergence auto- and cross-power spectrum  $\ell(\ell + 1)/(2\pi)P_{\kappa,ij}(\ell)$  for two redshift bins  $i,j$  with redshift ranges  $z = [0.5; 0.7]$ , and  $[0.9; 1.1]$ , respectively. Solid (dashed) lines correspond to the non-linear (linear) model. (b) Derivatives  $d \log P_\kappa / d \log p_k$  of the convergence power spectrum with respect to various cosmological parameters  $p_k$ , as indicated in the figure. The corresponding redshift bin is  $[0.9; 1.1]$ .

# GG, II & GI

---

*Besides noise, there are three contributions to the second order shear statistics (correlation functions or power spectra).*

*The **GG** or gravity-gravity correlations come from the gravitational lensing. This is what we have been studying.*

*The **II** or intrinsic-intrinsic correlations come from the intrinsic alignment of galaxies. This is usually considered a systematic error. This can be somewhat mitigated, at the expense of signal-to-noise, by separating the sources into groups that are separated in redshift and then looking for only correlations between these groups.*

*The **GI** or gravity-intrinsic correlations come from the alignment of galaxy shapes with the gravitational field. Correlations between sources at different redshifts (distances) would normally be attributed to lensing from mass in the foreground of both galaxies, but the mass around the lower redshift source will lens the other and effect the intrinsic ellipticity of the lower redshift galaxy. This will produce a false signal.*

$$C_l^{\text{total}} = C_{\text{GG}}^{ij}(\ell) + C_{\text{GI}}^{ij}(\ell) + C_{\text{IG}}^{ji}(\ell) + C_{\text{II}}^{ij}(\ell).$$

*A model for these contributions the observed shear is*

$$\epsilon^{ob} = \gamma_I + \gamma_G + \epsilon_o$$

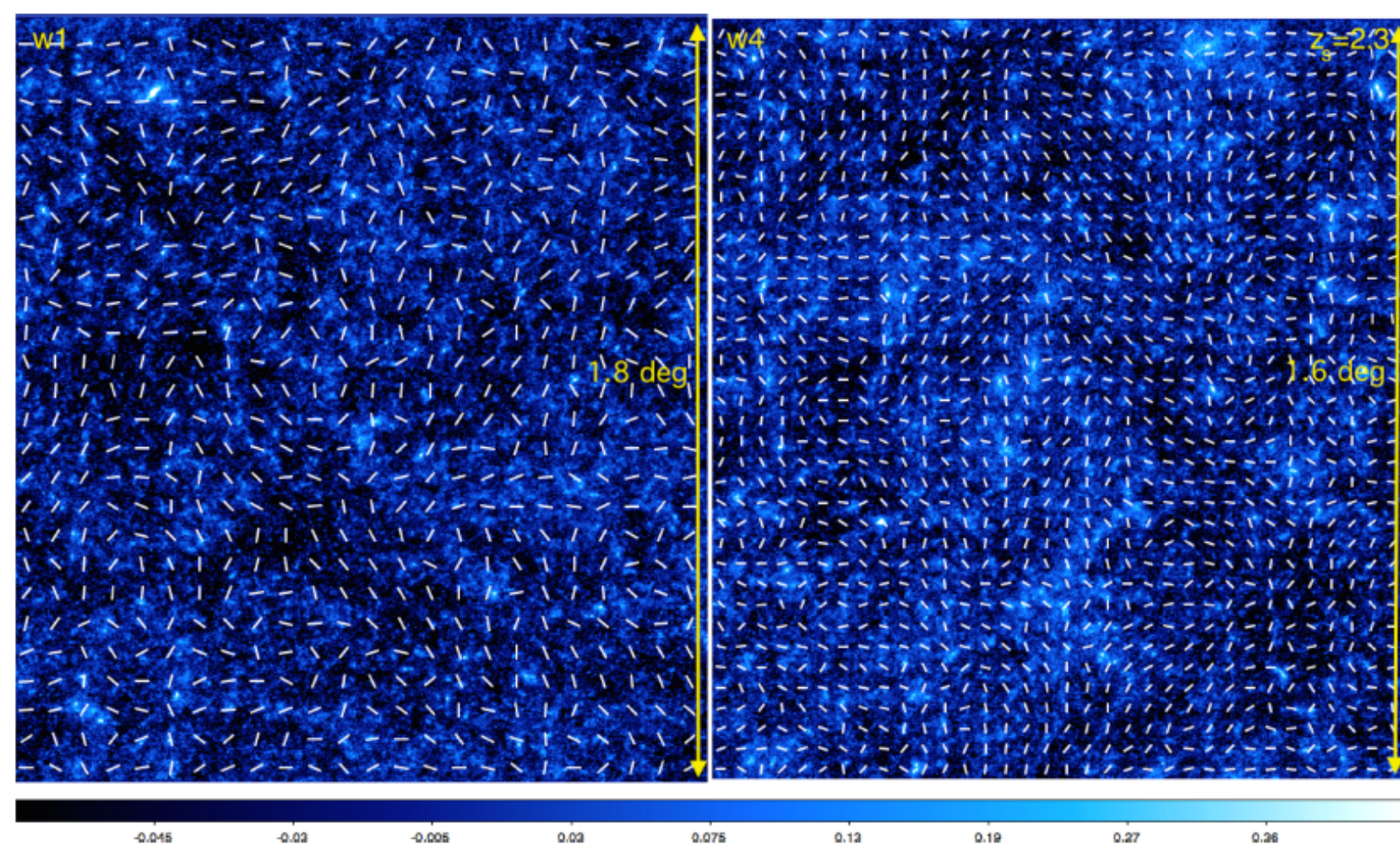
*gravitational shear*

*correlated intrinsic ellipticity*

*uncorrelated intrinsic ellipticity*

*The power spectrum between redshift bins including these terms will be*

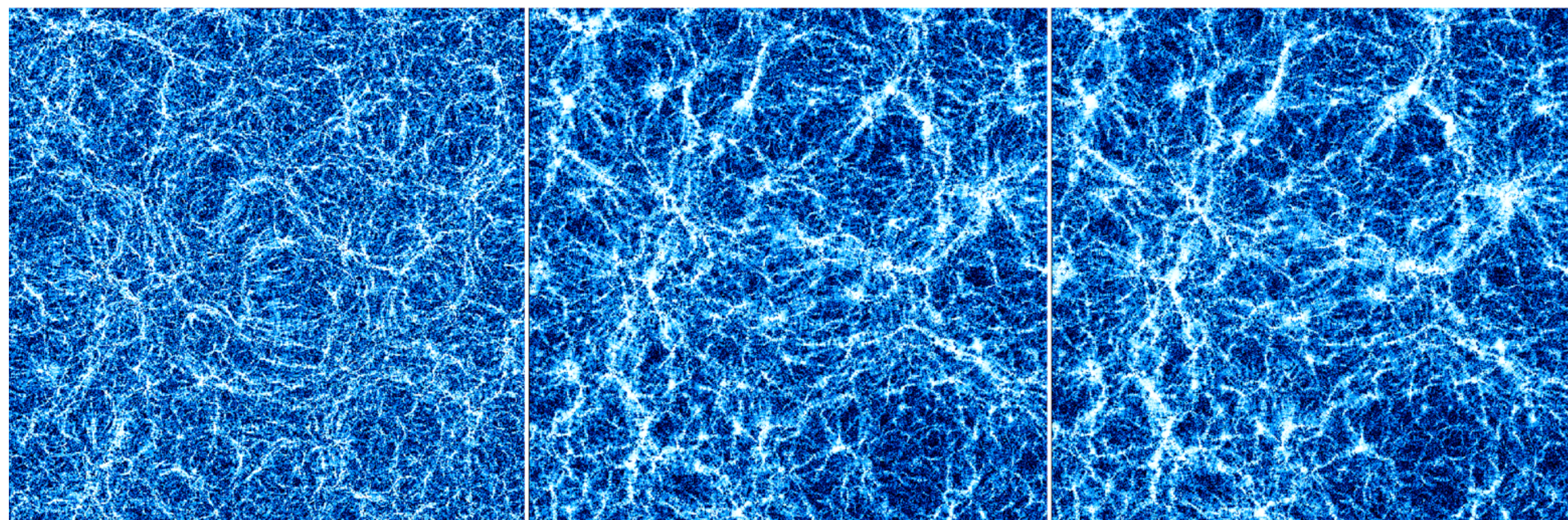
$$C_l^{\text{total}} = C_{\text{GG}}^{ij}(\ell) + C_{\text{GI}}^{ij}(\ell) + C_{\text{IG}}^{ji}(\ell) + C_{\text{II}}^{ij}(\ell).$$

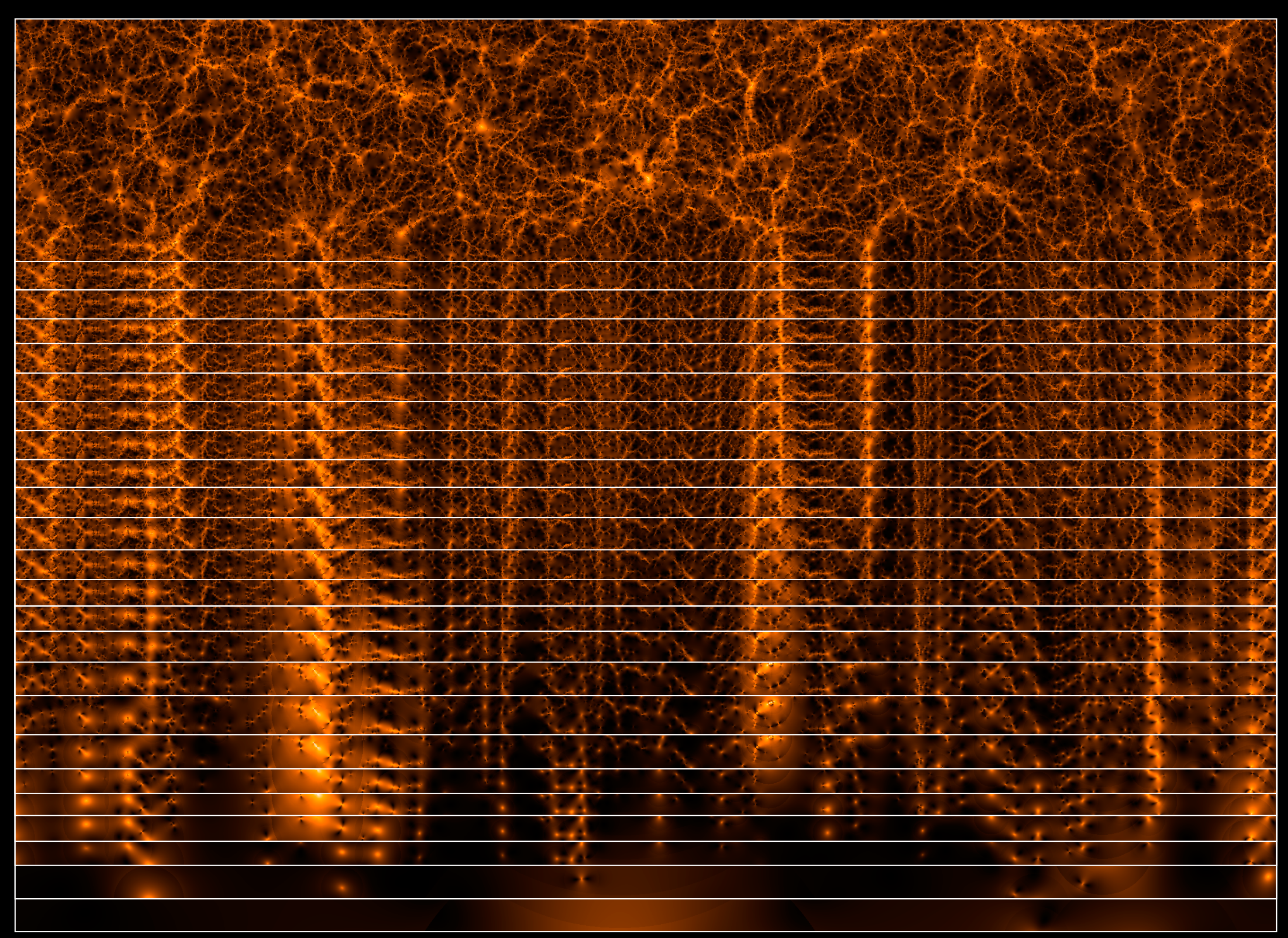


Convergence maps with shear  
overlaid

From ray-tracing simulation  
using the MultiDark cosmological simulation  
Giocoli et al. 2016

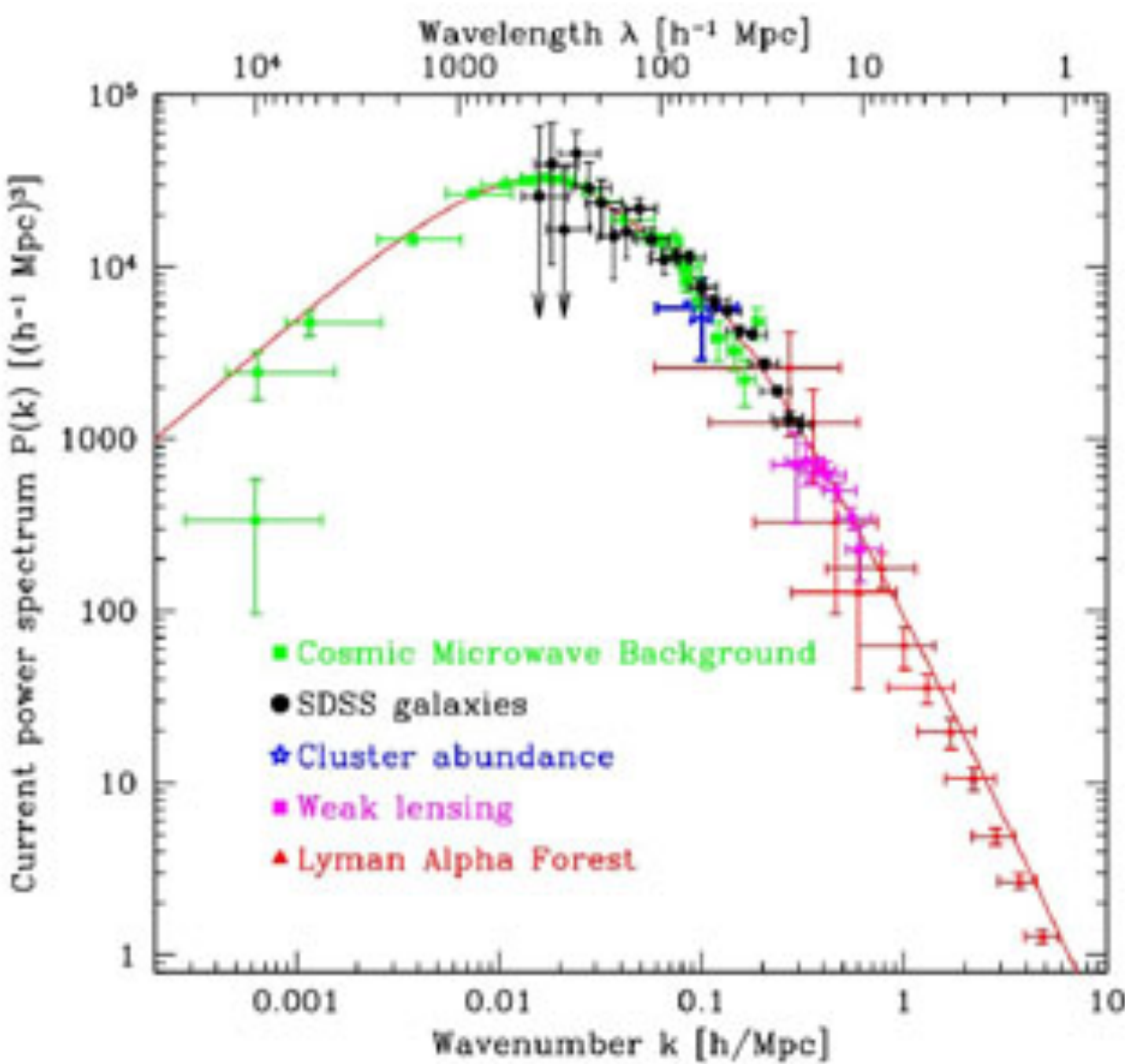
maps of the magnitude of the shear





# LENSING TOMOGRAPHY

---



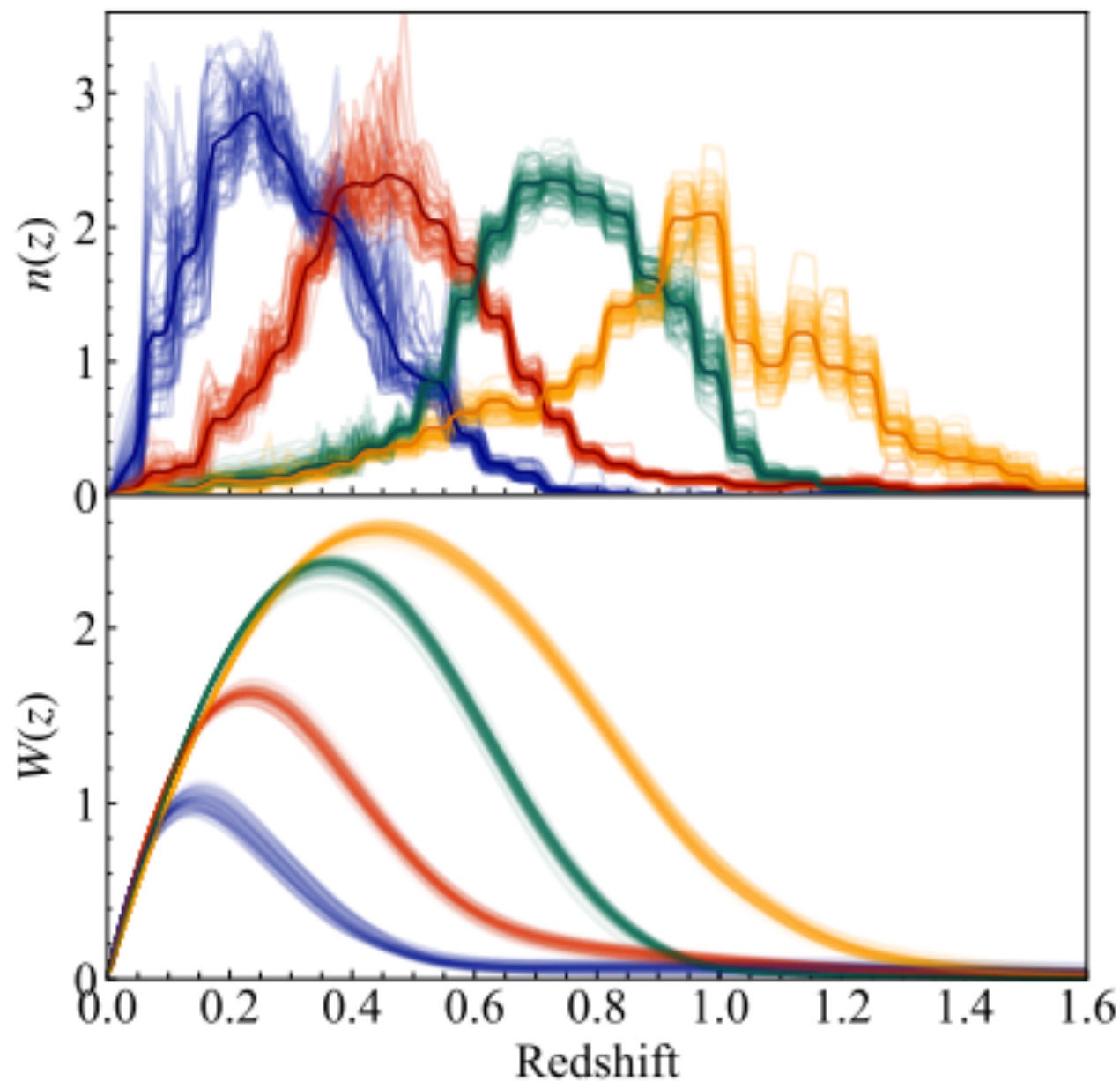
# COSMIC SHEAR CORRELATION FUNCTIONS

---

*DES - Dark Energy Survey Cosmic shear results*

*100 million source galaxies over 4,000 square degrees separated into four redshift bins*

*Source redshift distributions*



*weak lensing window  
functions for the different  
source bins*

# COSMIC SHEAR CORRELATION FUNCTIONS

Amon et al. 2021

*DES - Dark Energy Survey*

*the shear correlation and cross-correlation functions relative to theory for different source redshift bins.*

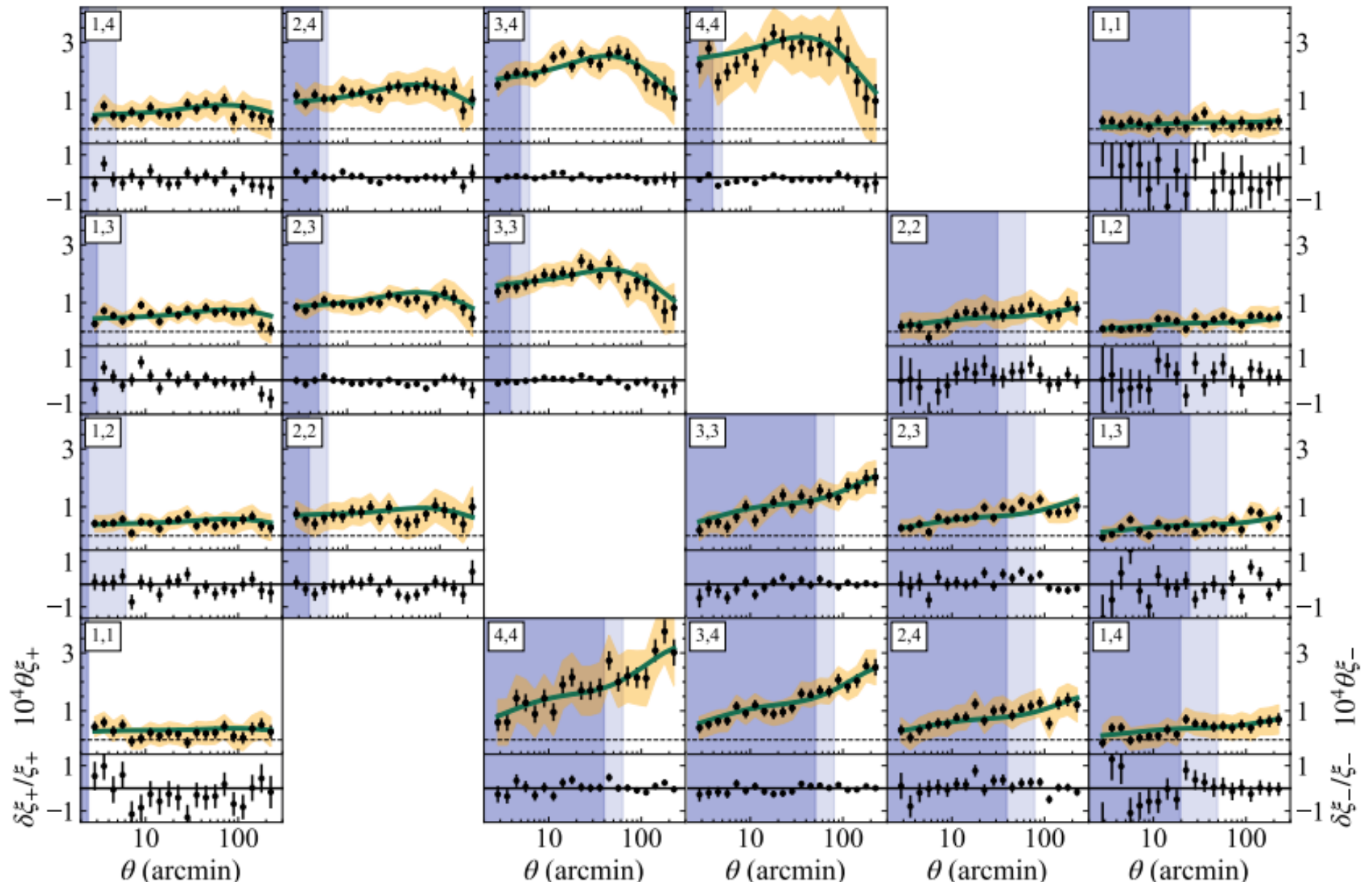


FIG. 3: Measured tomographic DES Y3 cosmic shear two-point correlation functions:  $\xi_+(\theta)$  (left) and  $\xi_-(\theta)$  (right), scaled by the angular separation,  $\theta$ , to emphasize differences relative to the best-fit model (upper panels). The correlation functions are measured for each redshift bin pair, indicated by the label and the error bar represents the square root of the diagonal of the analytic covariance matrix. The best-fit  $\Lambda$ CDM theoretical prediction from the cosmic shear-only tomographic analysis is denoted by a green line. Scales excluded from the analysis, due to their sensitivity to small-scale systematics, are shaded in light blue for the *Fiducial* analysis and darker blue for the  $\Lambda$ CDM-*Optimized* analysis. The signal-to-noise of the measurement is 40 using all angular scales and 27 (31) using the Fiducial ( $\Lambda$ CDM-Optimized) scale-selection. For comparison, the yellow shaded region shows the Y1 uncertainty, with a factor of  $\sim \sqrt{2}$  lower signal-to-noise. The lower panels plot the fractional difference between the measurements and best-fit,  $\delta\xi_{\pm}/\xi_{\pm} = (\xi_{\pm} - \xi_{\pm}^{\text{theory}})/\xi_{\pm}^{\text{theory}}$ . We find that the  $\chi^2$  per effective d.o.f of the  $\Lambda$ CDM model is  $237.7/222.2 = 1.07$ , and the  $p$ -value is 0.223.

# OBSERVATIONS

---

*Weak lensing surveys, to lowest order, measure a combination of cosmological parameters given by*

$$S_8 = \sigma_8 \left( \frac{\Omega_m}{0.3} \right)^\alpha$$

matter density  
power spectrum  
normalisation

$$\alpha \simeq 0.5$$

*Weakly depending on the redshift distribution of sources.*

# COSMIC SHEAR COSMOLOGICAL CONSTRAINTS

---

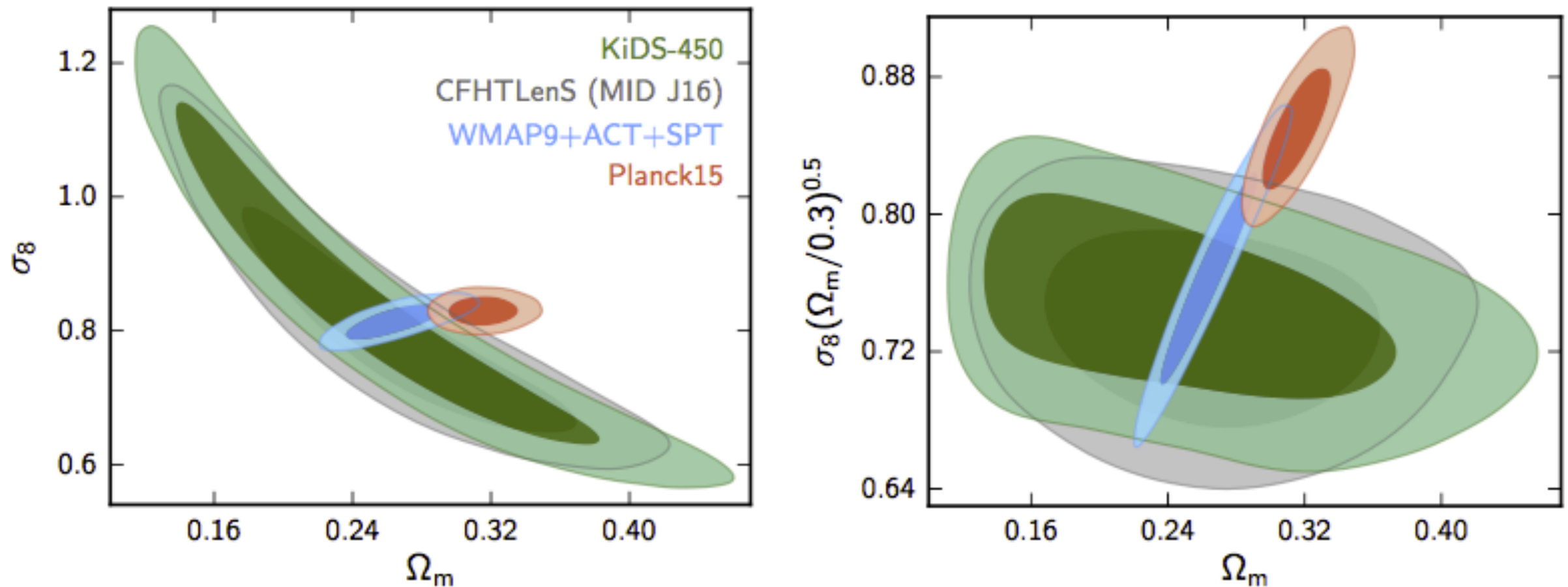


**Figure 6.** Marginalized posterior contours (inner 68% CL, outer 95% CL) in the  $\Omega_m$ - $\sigma_8$  plane (left) and  $\Omega_m$ - $S_8$  plane (right) from the present work (green), CFHTLenS (grey), pre-Planck CMB measurements (blue), and Planck 2015 (orange). Note that the horizontal extent of the confidence contours of the lensing measurements is sensitive to the choice of the prior on the scalar spectrum amplitude  $A_s$ . The CFHTLenS results are based on a more informative prior on  $A_s$  artificially shortening the contour along the degeneracy direction.

*Hildebrandt, et al. 2016*

# COSMIC SHEAR COSMOLOGICAL CONSTRAINTS

---

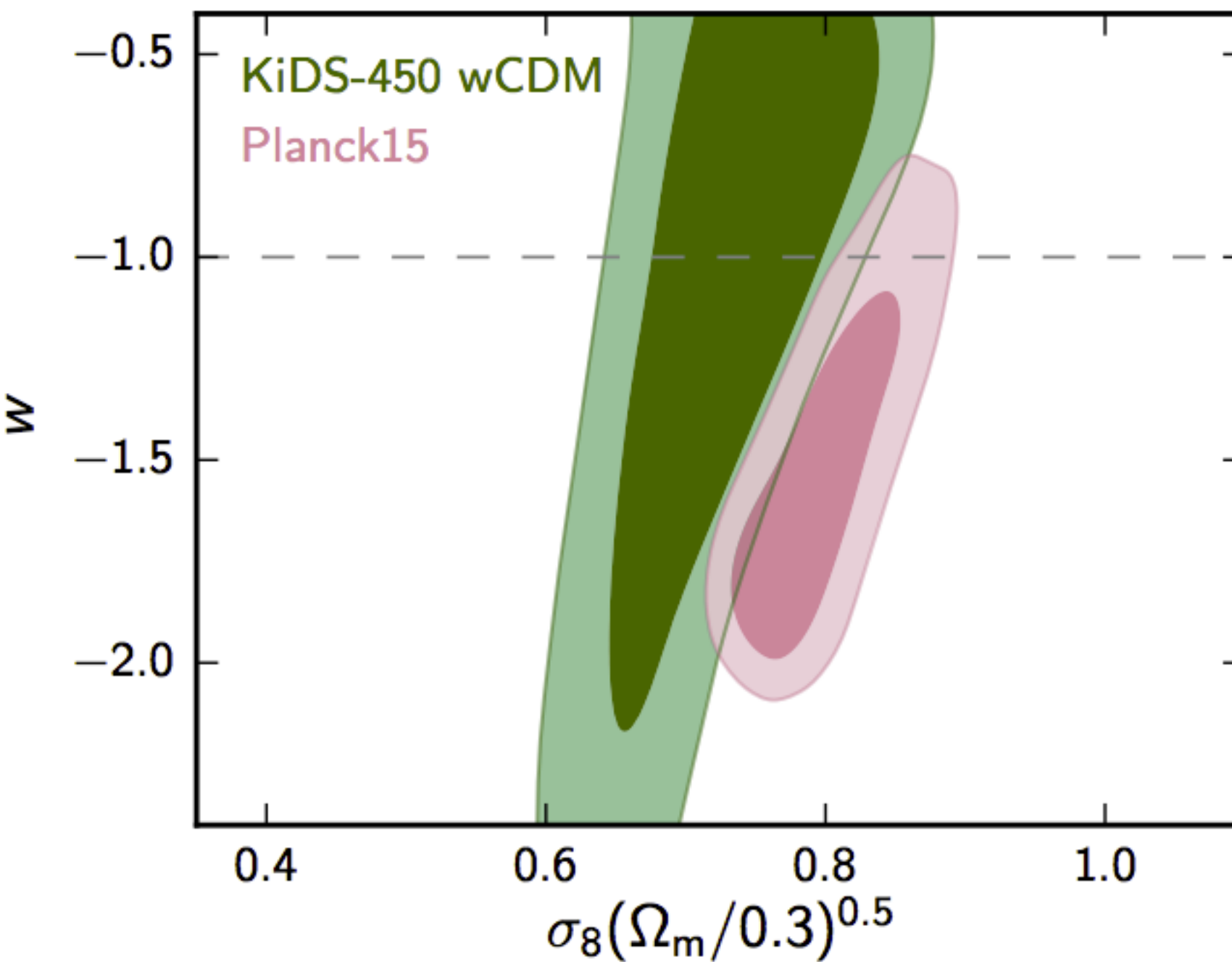
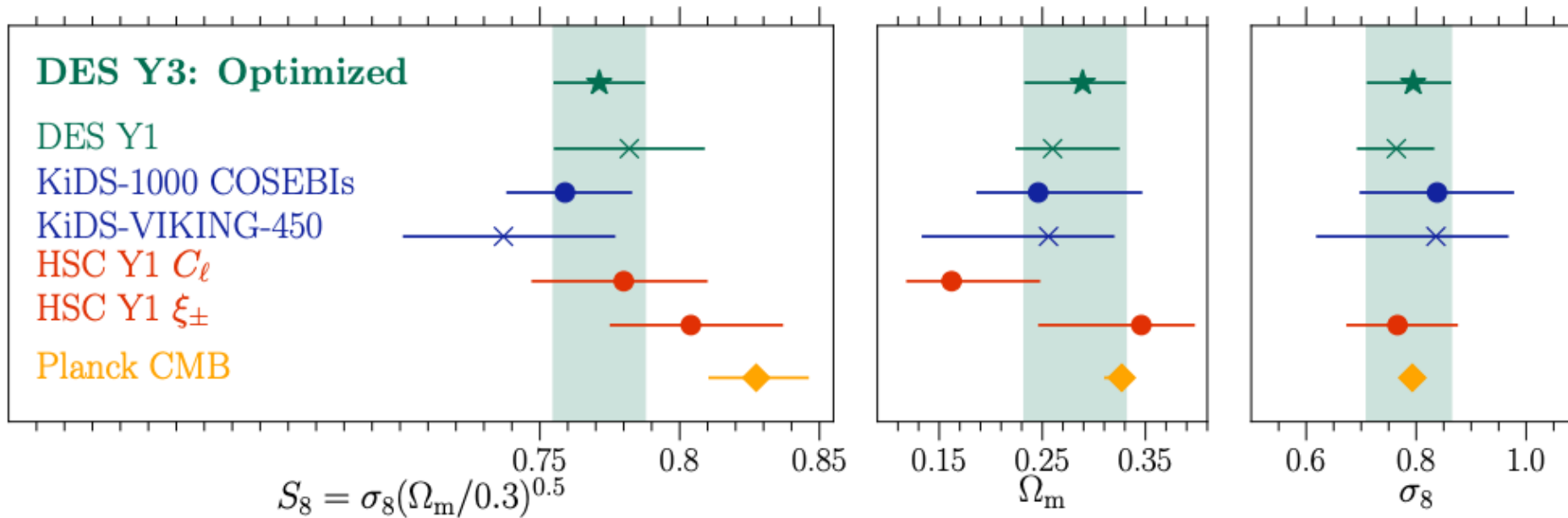
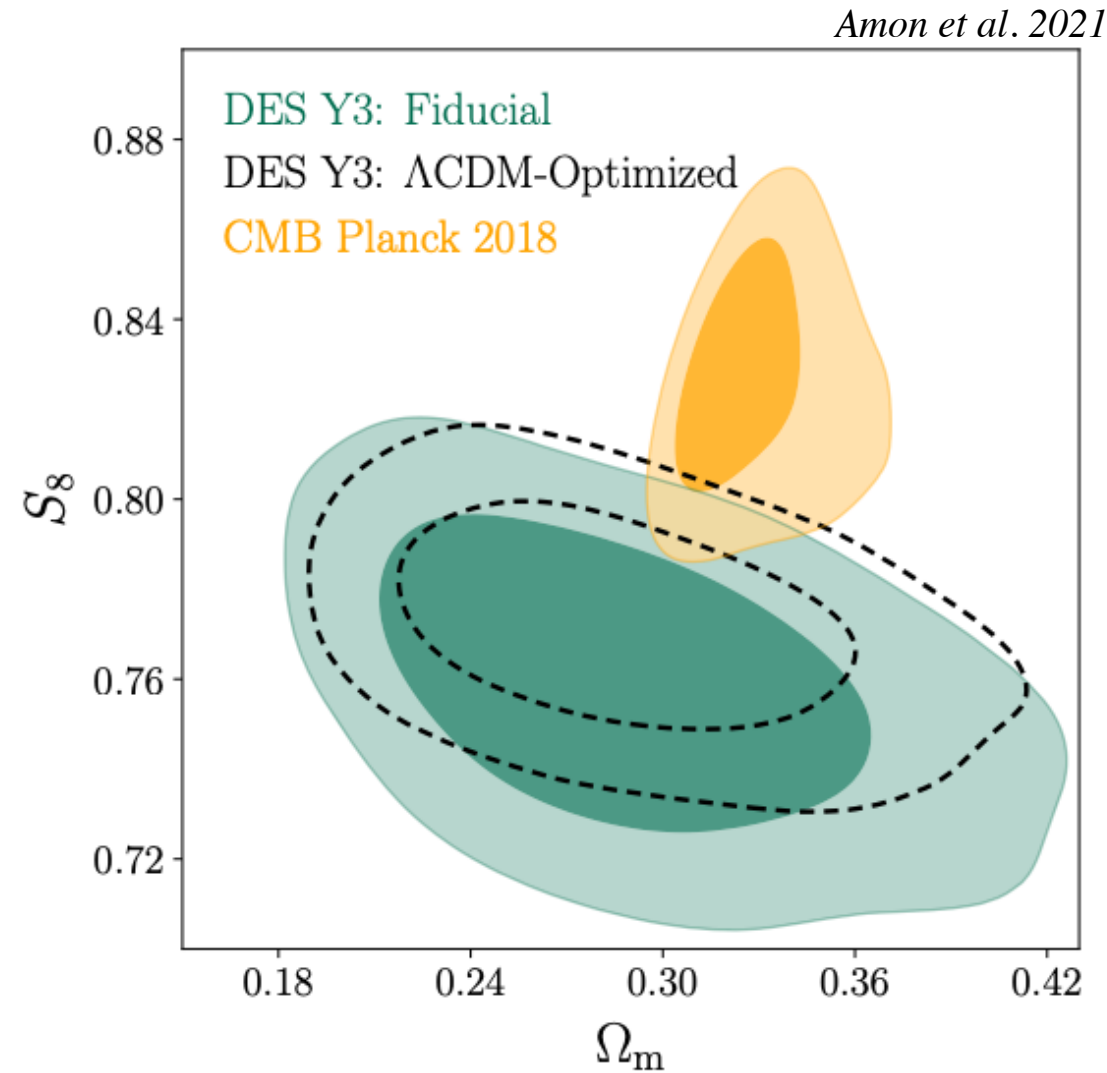
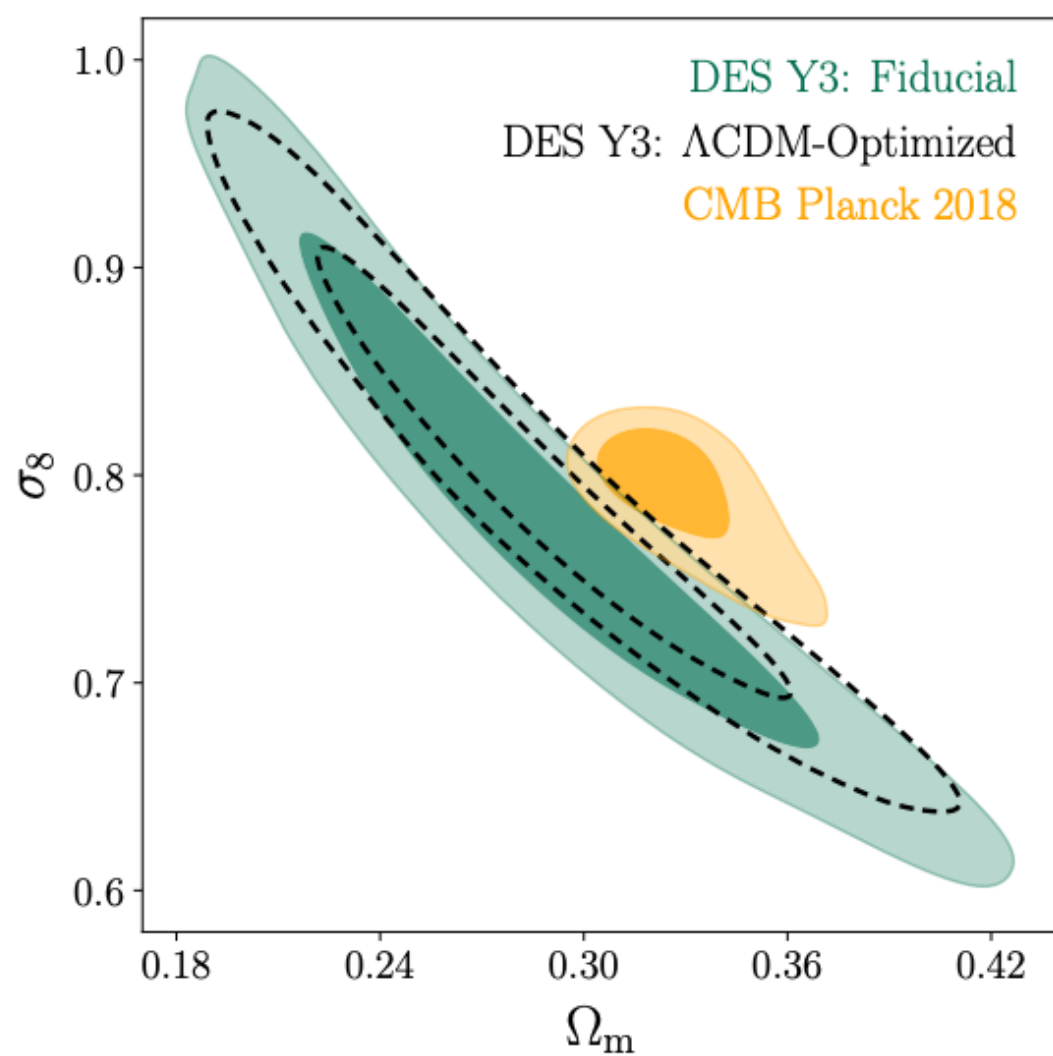


**Figure 9.** Marginalized posterior contours (inner 68% CL, outer 95% CL) in the  $S_8$ - $w$  plane from KiDS-450 (green) and Planck 2015 (pink).

# COSMIC SHEAR COSMOLOGICAL CONSTRAINTS



Amon et al. 2021

# COSMIC SHEAR COSMOLOGICAL CONSTRAINTS

$$S_8 = 0.783^{+0.021}_{-0.025}$$



DES Y1 gg lensing + cosmic shear + angular correlation function

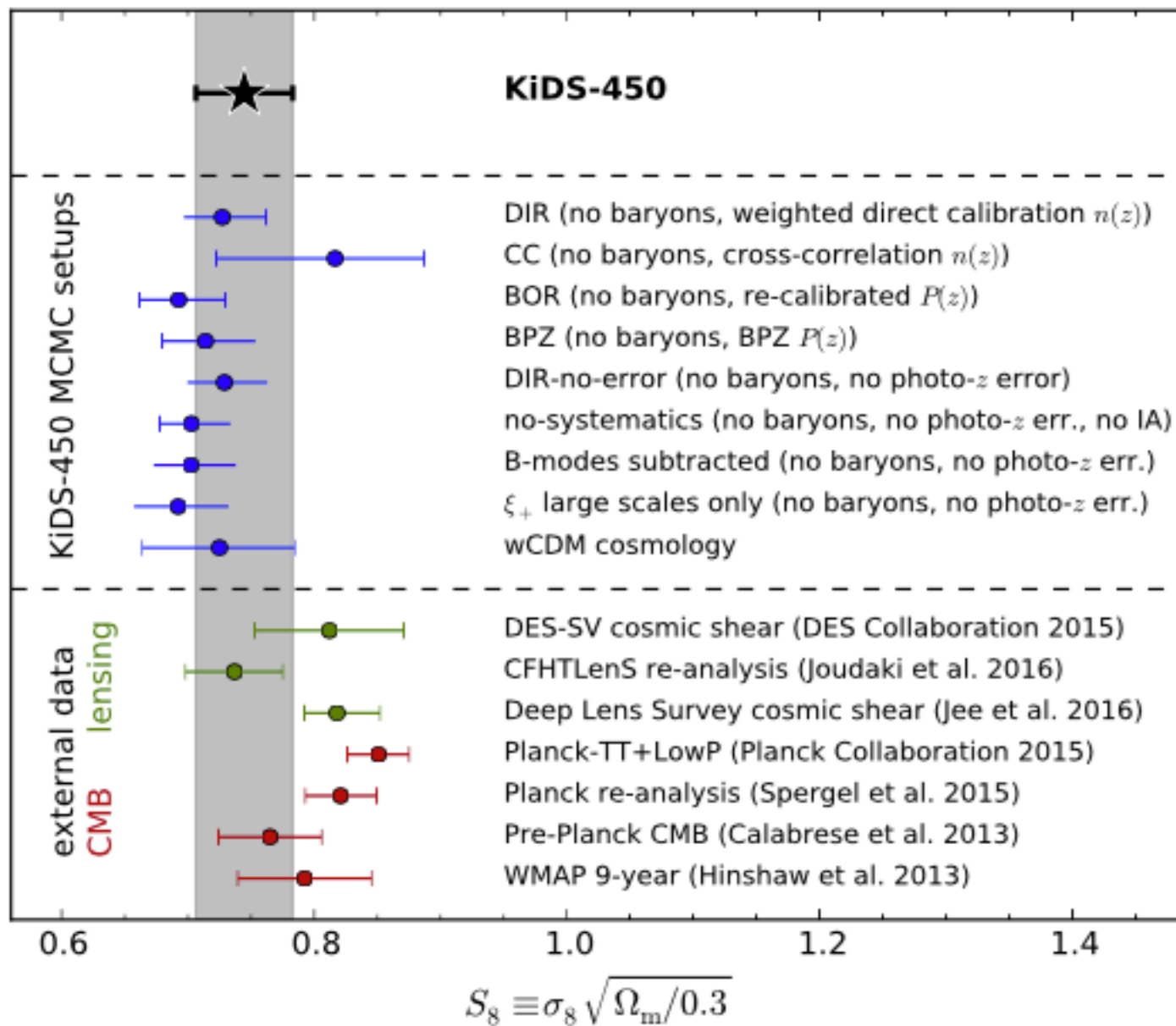
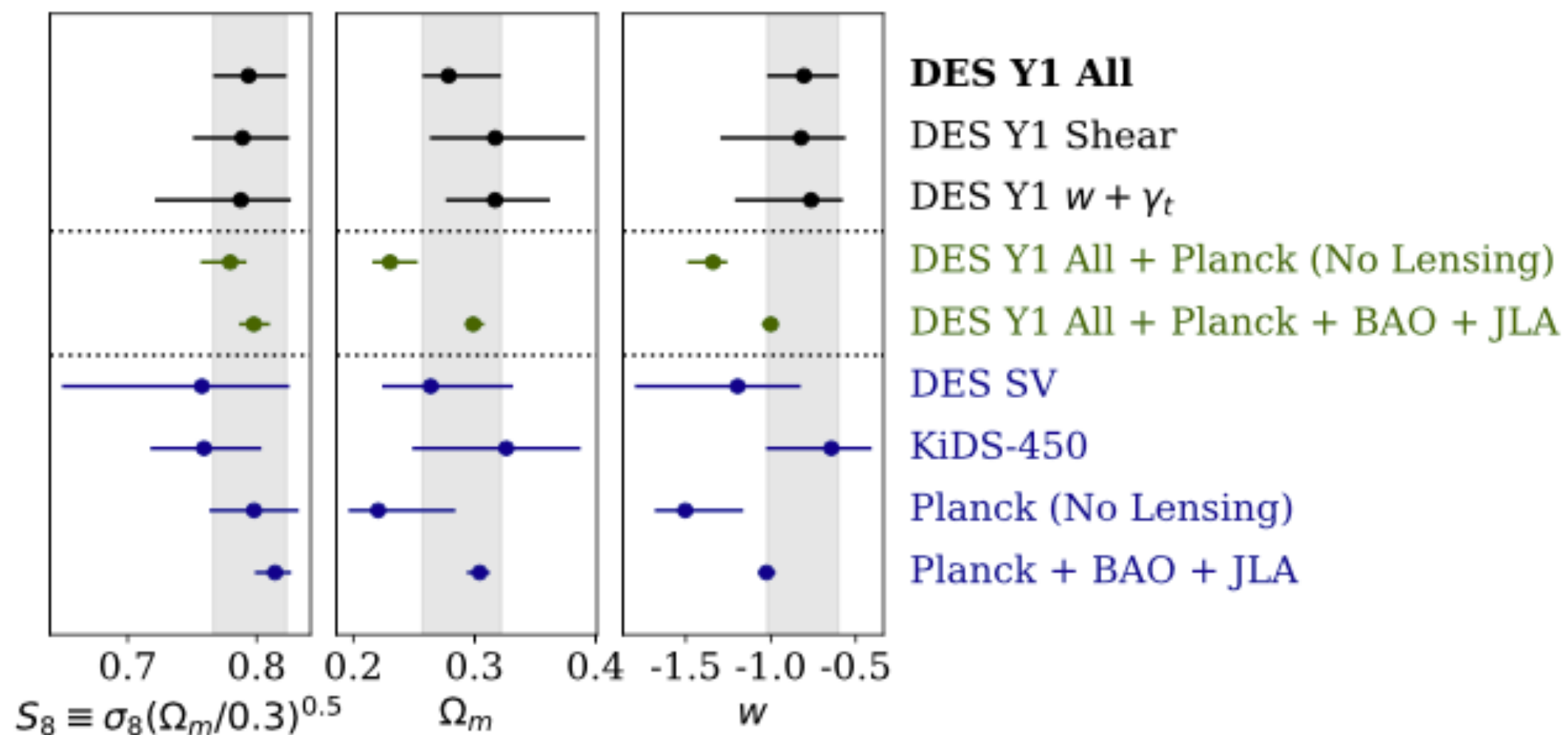


**Figure 10.** Constraints on  $S_8$  for the different runs considered in the KiDS-450 analysis as well as several literature measurements. The grey band indicates the  $1\sigma$  constraints from our primary analysis. Note that most of the runs which test for systematic errors (blue data points) switch off some of the astrophysical or redshift systematics. Hence not all data points shown here are fully comparable. For numerical values of the plotted data points see Table F1.

# COSMIC SHEAR COSMOLOGICAL CONSTRAINTS

---

DES Y1



Abbott, et al. 2017

*Observations*

# COSMIC SHEAR COSMOLOGICAL CONSTRAINTS

Future :

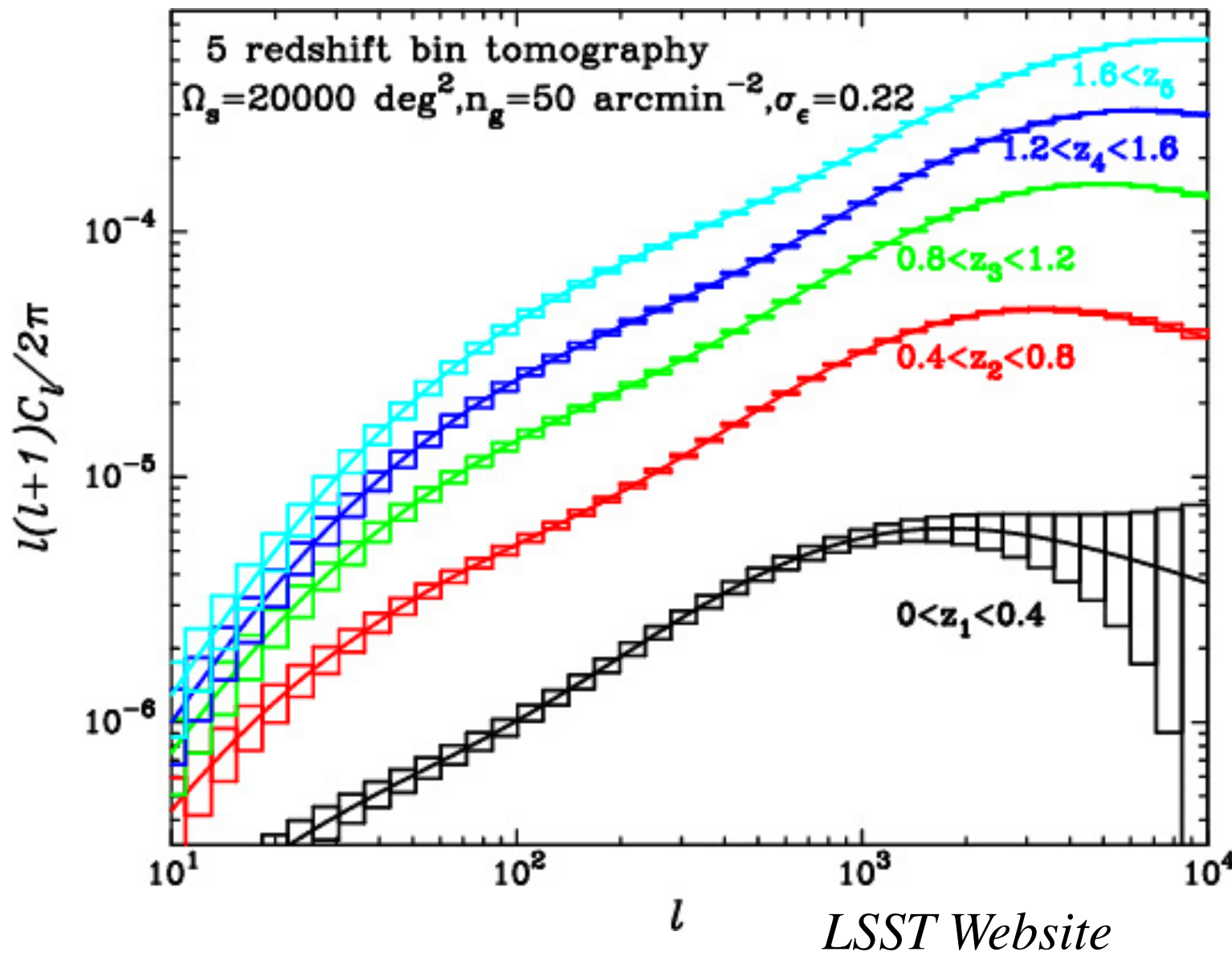
*Hyper SuprimeCam (HSC)*

*Large Synoptic Survey Telescope (LSST)*

*Wide Field Infrared Survey Tel. (WFIRST)*

*Euclid*

*Convergence Power Spectra for multiple source redshift bins*



*With redshift information, and enough galaxies, the shear power spectrum can be measured as a function of source redshift.*

*The redshifts for so many galaxies need to be measured by photometric redshifts.*

*This will probe the evolution in the energy densities of the universe as a function of redshift.*